Biochar amendment combined with partial root-zone drying irrigation alleviates salinity stress and improves root morphology and water use efficiency in cotton plant

Science of the Total Environment

Hou, Jingxiang; Wan, Heng; Liang, Kehao; Cui, Bingjing; Ma, Yingying et al

https://doi.org/10.1016/j.scitotenv.2023.166978

Science of the Total Environment 904 (2023) 166978

Contents lists available at ScienceDirect

Science of the Total Environment

journal homepage: www.elsevier.com/locate/scitotenv

Biochar amendment combined with partial root-zone drying irrigation alleviates salinity stress and improves root morphology and water use efficiency in cotton plant

Jingxiang Hou [a,b,c], Heng Wan [a,c,d], Kehao Liang [b], Bingjing Cui [a,b,c], Yingying Ma [e], Yiting Chen [b], Jie Liu [a,c], Yin Wang [f], Xuezhi Liu [g], Jiarui Zhang [a,c], Zhenhua Wei [a,c,*], Fulai Liu [b,**]

[a] College of Water Resources and Architectural Engineering, Northwest A&F University, Weihui Road 23, 712100 Yangling, Shaanxi, China
[b] Department of Plant and Environmental Science, Faculty of Science, University of Copenhagen, Højbakkegård Allé 13, DK-2630 Tåstrup, Denmark
[c] Key Laboratory of Agricultural Soil and Water Engineering in Arid and Semiarid Areas, Ministry of Education, Northwest A&F University, Yangling, Shaanxi 712100, China
[d] Soil Physics and Land Management Group, Wageningen University, P.O. Box 47, Wageningen, 6700 AA, Netherlands
[e] School of Ecology and Environment, Northwestern Polytechnical University, Xi'an, Shaanxi 710129, China
[f] College of Resources and Environmental Sciences, Jilin Agricultural University, Changchun 130118, Jilin, China
[g] School of Civil and Hydraulic Engineering, Ningxia University, Yinchuan 750021, China

HIGHLIGHTS

- The adsorption capacity of wheat straw biochar (WSP) for Na^+ was higher than that of softwood biochar.
- Biochar amendment reduced Na^+ concentration, increased K^+ concentration, and improved root morphology of cotton plants.
- WSP combined with alternate partial root-zone drying irrigation increased the salt tolerance and WUE of cotton plants.

GRAPHICAL ABSTRACT

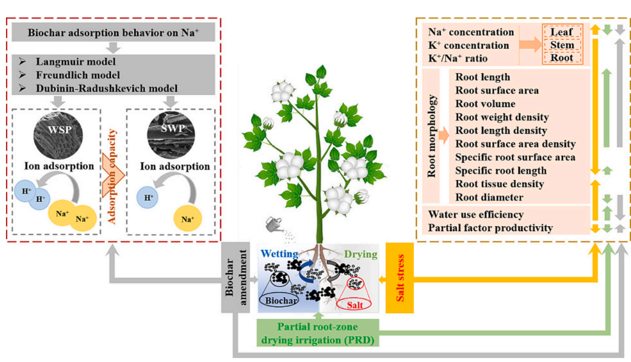

ARTICLE INFO

Editor: Zhaozhong Feng

Keywords:
Adsorption isothermal model

ABSTRACT

An adsorption experiment and a pot experiment were executed in order to explore the mechanisms by which biochar amendment in combination with reduced irrigation affects sodium and potassium uptake, root morphology, water use efficiency, and salinity tolerance of cotton plants. In the adsorption experiment, ten NaCl concentration gradients (0, 50, 100, 150, 200, 250, 300, 350, 400, and 500 mM) were set for testing isotherm

* Correspondence to: Z. Wei, College of Water Resources and Architectural Engineering, Northwest A&F University, Weihui Road 23, 712100 Yangling, Shaanxi, China.
** Correspondence to: F. Liu, Department of Plant and Environmental Science, Faculty of Science, University of Copenhagen, Højbakkegård Allé 13, DK-2630 Tåstrup, Denmark.
E-mail addresses: hnpdswzh@163.com (Z. Wei), fl@plen.ku.dk (F. Liu).

https://doi.org/10.1016/j.scitotenv.2023.166978
Received 23 June 2023; Received in revised form 4 September 2023; Accepted 8 September 2023
Available online 11 September 2023

Biochar
NaCl
Partial root-zone drying irrigation
Water use efficiency

adsorption of Na^+ by biochar. It was found that the isotherms of Na^+ adsorption by wheat straw biochar (WSP) and softwood biochar (SWP) were in accordance with the Langmuir isotherm model, and the Na^+ adsorption ability of WSP (55.20 mg g^{-1}) was superior to that of SWP (47.38 mg g^{-1}). The pot experiment consisted three factors, viz., three biochar amendments (no biochar, WSP, and SWP), three irrigation strategies (deficit irrigation, partial root-zone drying irrigation – PRD, full irrigation), and two NaCl concentrations gradients (0 mM and 200 mM). The findings indicated that salinity stress lowered K^+ concentration, root length, root surface area, and root volume (RV), but increased Na^+ concentration, root average diameter, and root tissue density. However, biochar amendment decreased Na^+ concentration, increased K^+ concentration, and improved root morphology. In particular, the combination of WSP and PRD increased K^+/Na^+ ratio, RV, root weight density, root surface area density, water use efficiency, and partial factor productivity under salt stress, which can be a promising strategy to cope with drought and salinity stress in cotton production.

1. Introduction

As an important fiber and cash crop, cotton (*Gossypium hirsutum* L.) grows mainly in tropical and subtropical areas of more than eighty countries around the world (Abdelraheem et al., 2019; Li et al., 2023). Meanwhile, as the second major producer of cotton worldwide, China manufactures 23 % of the world's cotton fiber (Abdelraheem et al., 2019; Wang et al., 2022). Moreover, cotton cultivation is an important source of economic income for many smallholder producers in China (Li et al., 2023; Wang et al., 2022). However, salinity stress and water scarcity are currently the major limiting factors for cotton cultivation in arid and sub-arid areas (Abdelraheem et al., 2019; Li et al., 2023). Therefore, it is urgent to find efficient water-saving irrigation technology and methods to alleviate salinity stress.

Salt stress has many detrimental effects on plant growth. For example, I) salinity can induce osmotic stress, thereby affecting the water uptake of the plant (Liang et al., 2018); II) salinity often induces ion toxicity, with higher Na^+ reducing plant photosynthesis and tending to lead to an imbalance of intracellular ions (Hannachi and Van Labeke, 2018). III) Salt stress can also lead to nutrient imbalance, especially by reducing the uptake of K^+, which is important for maintaining many physiological processes in the plant and therefore affects plant development (Kiani et al., 2017; Xiong et al., 2018). K^+ plays a vital function in the reversal of salinity stress, mainly by regulating intracellular ion homeostasis and antioxidant metabolism, which in turn influences the ROS scavenging process to alleviate the injury caused by salinity (Ahanger and Agarwal, 2017; Cakmak, 2005). In many species, K^+ supply can increase osmotic regulation and improve plant water relations (Ashraf et al., 2001; Sangakkara et al., 2000; Shabala and Pottosin, 2014). Especially, adequate K^+ supply is required to sustain the normal growth and function of roots under salinity stress (Wang et al., 2013). Therefore, limiting Na^+ absorption and lowering Na^+ concentration in plants, while reducing K^+ loss from the roots, is essential to improve salt resistance in plants (Liang et al., 2018; Sun et al., 2016; Xiong et al., 2018; Zhang et al., 2009; Zhang and Shi, 2013). Indeed, earlier researches have suggested that the proper K^+/Na^+ is necessary for the activation of cytoplasmic enzymes (Chakraborty et al., 2016; Ju et al., 2023; Zhang et al., 2018).

On the other hand, under stress conditions, the root system of the crop, as an organ in direct contact with the soil, can be significantly altered in its morphology (Yoshimura et al., 2008), thus affecting the uptake of water and nutrients (Djanaguiraman et al., 2018), which in turn has an impact on crop physiology and yield (Hamada et al., 2011; Ranjan et al., 2022; Zhou et al., 2021). In other words, due to the phenotypic plasticity of the root system, plants can regulate their root morphological traits and the direction of root growth to avoid salinity and drought stresses (Chun et al., 2021; Galvan-Ampudia and Testerink, 2011). Therefore, it is essential to examine the changes in the root morphology of plants under abiotic stress, which has significant implications for understanding the physiological response of the plants. At the same time, finding a method and strategy to alleviate salinity and drought stress is also imminent in order to cope with the environmental challenges that adversely affect crop growth and productivity.

It has been reported already that biochar amendment has the potential to mitigate drought and salinity stress (Akhtar et al., 2015b; Zhang et al., 2020). Biochar is a solid carbon-rich material derived from thermochemical transformation of biological matter under oxygen-limited or anaerobic conditions (Hussain et al., 2020). During the process of pyrolysis, a large number of pore structures and functional groups are established on the biochar surface (Sun et al., 2021), allowing biochar amendment to improve soil fertility, retain nutrients, stimulate microbial activity, and immobilize inorganic or organic pollutants (Ruan et al., 2019). Moreover, previous reports generally suggest that the porosity, huge surface area, and functional group-rich properties of biochar give it the ability to adsorb large amounts of inorganic ions (Leng et al., 2022; Mahmoud et al., 2020; Xu et al., 2023). Also, biochar amendment can modify the physicochemical characteristics of soil minerals (Cai et al., 2022); for example, biochar amendment can change the surface area, and ion-exchange capacity through ion-exchange interaction of interlayer cations or anions, or through hydroxyl complexation (Jing et al., 2022; Wang et al., 2021b). Further, biochar amendment can decrease the concentration of reactive oxygen species like $O_2^{\bullet -}$ and H_2O_2 (Jiang and Zhang, 2001; Kim et al., 2016) by lowering the Na^+ concentration in plant tissues, and thus effectively mitigate oxidative stress (Akhtar et al., 2015a; Akhtar et al., 2015b; Akhtar et al., 2015c). In addition, biochar amendment can raise the soil potassium content to meet the nutrient demand of plants, indicating that biochar can serve as an alternative to chemical potassium fertilizers to some extent and reduce the risk to the environment posed by chemical potassium fertilizers (Wu et al., 2019).

In addition to biochar amendment, salinity stress can also be ameliorated by some irrigation practices (Munns, 2002), such as partial root-zone drying irrigation (PRD), which can mitigate salinity stress in addition to enhancing crop water use efficiency (WUE) (Hou et al., 2023; Kong et al., 2016; Kong et al., 2017). The advantage of the PRD strategy is that it allows roots on the desiccated side to produce abscisic acid (ABA) to reduce the stomatal opening and thus the luxurious transpiration of the plant, increasing the WUE of the crop, while roots on the wetted side maintain the normal growth of the crop (Davies et al., 2002; Kang and Zhang, 2004; Liu et al., 2006; Wei et al., 2018). Moreover, PRD strategy caused inhomogeneous salt distribution in soil solution, which induced the expression of Na^+ efflux genes (e.g., *SOS1, SOS2, PMA1,* and *PMA2*), improved the ability of plant roots to release Na^+, lowered the Na^+ content of roots and plants, hence mitigating salt stress (Kong et al., 2012, 2016; Kong et al., 2017).

Although there have been some reports that biochar amendment can mitigate salinity stress and facilitate crop performance (Drake et al., 2015; Hammer et al., 2015; Huang et al., 2019; Ju et al., 2021; Mehmood et al., 2020; Tang et al., 2020; Thomas et al., 2013; Yang et al., 2020; Zhang et al., 2019b), the underlying mechanisms have not been fully understood. Moreover, current studies on the sorption properties of biochar have mainly focused on heavy metal ions (e.g., Cd^{2+}, Pb^{2+}, Zn^{2+}) (Deliyanni et al., 2012; Liu et al., 2022a; Lu et al., 2012; Soria et al., 2020), few studies have investigated the mechanism of Na^+ sorption by different types of biochars. Moreover, studies on biochar application in combination with PRD strategy to alleviate salinity stress and improve root morphology and reducing Na^+ uptake in cotton plants have not yet been published. Therefore, a greenhouse pot experiment and an isothermal sorption test of biochar on Na^+ was conducted to survey the effects of different types of biochar coupled with PRD on root morphology, Na^+ and K^+ uptake, and water use efficiency, and to elucidate the sorption mechanism of biochar on Na^+. It was hypothesized that wheat straw biochar coupled with PRD could significantly reduce Na^+ uptake, improve root morphology, water use efficiency, and partial factor productivity in cotton plants.

2. Materials and methods

2.1. Experimental materials

The soil chosen for the experiment was collected from a local farm in Yangling, Shaanxi, China. The soil consisted of 85 % silt, 8 % clay, and 7 % sand and is classified as silt according to USDA classification. Biochar was sourced from the Biochar Research Centre in the UK and was generated by the pyrolysis of raw materials of soft wood and wheat straw at 550 °C under anaerobic conditions, labeled SWP and WSP, respectively. Later, the biochar was ground into a powder. And, the soil also passed through a 0.5 cm sieve after air-drying for subsequent use. The physical and chemical properties of the soil and biochar are detailed in Table 1.

2.2. Sodium adsorption experiment

2.2.1. Sodium adsorption isotherm studies

The sodium adsorption experiment was carried out for WSP and SWP biochar. 0.2 g of biochar was placed in a 25-mL centrifuge tube, followed by the addition of 20 mL of NaCl solutions with concentration gradients of 0, 50, 100, 150, 200, 250, 300, 350, 400, and 500 mM, respectively. All tubes were vibrated for 24 h at 25 ± 1 °C. After equilibration, all tubes were subjected to centrifugation at 4000 r/min for 5 min and the supernatant was filtered through filter paper (whatman 40). The Na^+ concentration of the filtrate was assayed using an Inductive Coupled Plasma Emission Spectrometer (ICP, MS6880, China). The adsorption amount of Na^+ by biochar was computed using Eq. (1) according to Akhtar et al. (2015a). The adsorption experiment contained two types of biochar, 10 concentrations of NaCl solution, three replicates, and a total of 60 centrifuge tubes.

$$q_e = \frac{(C_i - C_e) \times V}{m} \tag{1}$$

where, q_e (mg g^{-1}) denotes the adsorption amount at the equilibrium; C_i and C_e denote the Na^+ concentration in the solution at the beginning state and at equilibrium, respectively; V denotes the solution volume (L); and m denotes the mass of biochar (g).

Table 1
Physical and chemical properties of soils and biochar.

Properties	Soil	WSP	SWP
EC, μS cm^{-1}	360	1700	90
pH	7.72	9.94	7.91
CEC, cmol + kg^{-1}	1.95	6.15	3.15
Total N, g kg^{-1}	0.46	13.9	<1
Total K, g kg^{-1}	24.24	15.6	2.5
Total P, g kg^{-1}	0.59	1.4	0.6
Total C, g kg^{-1}	17.79	682.6	855.2
Available K, mg kg^{-1}	86.33	–	–
C/N ratio	38.67	49.11	<855.2
C stability, %	–	96.51	69.62
Zinc, mg kg^{-1}	–	10.50	25.71
Copper, mg kg^{-1}	–	3.63	19.41
Cadmium, mg kg^{-1}	–	3.15	3.48
Nickel, mg kg^{-1}	–	1.00	3.30
Total surface area, m^2 g^{-1}	–	26.40	26.40
Total ash, %	–	21.25	1.25
Total pore volume, cm^3 g^{-1}	–	0.02	0.00
BET, m^2 g^{-1}	–	299	27.57

2.2.2. Adsorption isothermal model

To assess the adsorption characteristics of biochar on Na^+, the maximum adsorption capacity, and the adsorption mechanism of Na^+, the Langmuir isotherm model (Langmuir, 1918), Freundlich isotherm model (Freundlich, 1907), and Dubinin-Radushkevich isotherm model (Dubinin, 1975) were assessed based on Eqs. (2), (3), (4), and (5), respectively.

$$q_e = \frac{K_l q_m C_e}{1 + K_l C_e} \tag{2}$$

where, q_e (mg g^{-1}) denotes the adsorption amount at the equilibrium; K_l (L mg^{-1}) is a constant of Langmuir, which is associated with the affinity of the binding site; q_m (mg g^{-1}) is the maximum adsorption capacity; C_e (mg L^{-1}) is the concentration of Na^+ in the equilibrium solution.

$$q_e = K_f C_e^{\frac{1}{n}} \tag{3}$$

where, K_f (L g^{-1}) is the Freundlich constant; n is the Freundlich exponent, which is associated with the adsorption intensity.

$$q_e = q_m \cdot exp\left\{ -\beta \cdot \left[RTln\left(1 + \frac{1}{C_e}\right) \right]^2 \right\} \tag{4}$$

$$E = \frac{1}{\sqrt{2\beta}} \tag{5}$$

where, q_e (mg g^{-1}) denotes the same as in Eq. (1); C_e (mg L^{-1}) is the same as in Eq. (2); q_m (mg g^{-1}) is the maximum sorption capacity; β (mol^2 KJ^{-2}) is the Dubinin-Radushkevich constant, which is associated with the adsorption energy; R is the universal gas constant (8.314 J mol^{-1} K^{-1}); and T (K) is the absolute temperature.

From β, the Gibbs free energy (E, kJ mol^{-1}) can be computed based on Eq. (5) according to Mane et al. (2007) for the purpose of differentiating the kind of adsorption process. When E is <8 kJ mol^{-1}, the adsorption process is a physical process, and when E is between 8 kJ $mol^{-1}$and 16 kJ mol^{-1}, it is a chemical process (Taha et al., 2016).

2.3. Pot experiment

The location of greenhouse pot trials was located at Northwest A&F University (34° 15′N, 108° 04′E) in Yangling, Shaanxi, China, starting in June 2020 and ending in January 2021. Prior to the trial start, biochar was mixed with soil at a 2 % (w/w) addition rate, and then the soil or mixture was packed into custom-made split-root pots with a packed soil weight of 18 kg. Meanwhile, 5.40 g KH_2PO_4 and 4.86 g urea were thoroughly incorporated into the soil of each pot to provide sufficient nutrients required for cotton growth. The split-root pot was a rectangular shape with a height of 40 cm and a length and width of 26 cm and 16 cm, respectively, and was divided equally into two compartments in the middle of the pot by a PVC divider with a groove. This groove (6 cm high and 3 cm long) was reserved for the purpose of transplanting the cotton seedlings there afterward. The bulk density and the water holding capacity (WHC) of the filled soil were1.20 g cm^{-3} and 25 %, respectively, and the WHC of the soil mixed with SWP and WSP was 26 % and 27 %, respectively. The permanent wilting point of the soil is 8 % (gravimetric). The cotton (*Gossypium hirsutum* L.) variety used in the experiment was Lumian No. 37 from China. Cotton seeds were first sown in seedling trays, and when they reached the 3–4 leaf stage, we selected uniformly growing cotton seedlings and transplanted them into split-root pots, one cotton seedling per pot. In order to avoid the influence of other factors, we did not treat the cotton seeds before sowing. At the time of transplanting, the principal roots of the cotton seedlings were separated into two equal portions using a scalpel, and the seedlings were then moved to the grooved position in the root-splitting pots. Subsequently, two probes were inserted into the two compartments to detect the soil water content (SWC) by TDR (Minitrase, USA). Furthermore, a 2 cm layer of perlite was placed on the soil top for minimal soil evaporation.

The pot experiment included a total of three factors, four replicates, and a total of 72 pots. Namely, the biochar amendment ([B]) mainly included wheat straw biochar (WSP), soft wood biochar (SWP) and no biochar amendment (CK); the irrigation regime ([IR]) mainly included deficit irrigation (DI), partial root-zone drying irrigation (PRD), full irrigation (FI); and the salt addition ([S]) consisted of two NaCl levels of 0 mM (S0) and 200 mM (S1). One month after the cotton seedlings were transplanted, salt treatment was started by randomly selecting half the number of cotton plants from 72 pots for salt addition as S1 treatment. The specific operation was to add 100 mL of NaCl solution to the pots every two days, 4.74 g NaCl each time, and to continue adding NaCl solution for 20 d, so that the NaCl concentration of the soil solution was 200 mM (i.e., the salt content of the soil is about 0.26 %) after the end of salt addition. After the end of the salt treatment, three irrigation treatments were applied to all cotton plants. Irrigation treatments were applied from 16:00 to 18:00 daily and maintained for a total of 100 d, i.e., throughout the budding, flowering & boll-setting, and boll-opening stages of cotton plant growth.

For all FI treatments, irrigation was applied up to 90 % of WHC. For the DI and PRD treatments, irrigation was applied at 70 % of the irrigation amount for each FI. The difference between the DI and PRD was that for DI both compartments of the pots were irrigated at a time, whereas for the PRD treatment only one compartment was irrigated until the soil water content of the other soil compartment dropped to 12 %, then the switch to irrigating the other compartment was initiated. Here we need to emphasize that the soil salinity has a huge impact on the monitoring of the TDR equipment, making it impossible to rely on the TDR for accurate monitoring of the SWC under S1. Therefore, we use the traditional weighing approach to detect the SWC for S1, and the TDR device is only used to detect the SWC under S0. Moreover, for the S0 treatment, we also use the weighing method to calibrate the TDR. As a result, we could not obtain the soil water content change curve for the PRD under S1, but for the irrigation conversion cycle of PRD under S1, we follow the corresponding irrigation cycle of PRD under S0. The variation curves of SWC during the irrigation treatment are described in Hou et al. (2023).

The environmental conditions during the treatment period for the pot experiment were monitored by a temperature & humidity measurement instrument (TH-Logger, China) in the greenhouse, see Fig. S1, mainly including temperature (T), relative humidity (RH), and vapor pressure deficiency (*V*PD).

2.4. Measurements and calculations

2.4.1. Surface morphology of biochar

The microscopic morphology of biochar was described using a scanning electron microscopy (SEM, TESCAN-MIRA, LMS, The Czech Republic). The biochar samples were coated with a thin gold layer and then measured at 15 kV according to Shen et al. (2017).

2.4.2. Fourier-transform infrared spectroscopy

Fourier-transform infrared spectroscopy (FTIR) was executed in order to identify the major functional groups on the surface of biochar. 2 mg biochar and 200 mg KBr were weighed and their mixture was made into a sample press at a pressure of 1 MPa, and then the samples were analyzed by FTIR (Thermo Scientific Nicolet iS5, America) at a solution of 2 cm^{-1} in the 4000–400 cm^{-1} range.

2.4.3. Na^+ and K^+ concentration of different organs of cotton plants

On January 21, the leaves, stems and roots were individually harvested and then dried to a stable weight in an oven at 75 °C. These dry samples were then milled into powder and sieved through a 0.25 mm mesh sieve. The Na^+ concentration in the leaves ($[Na^+]_{leaf}$), stems ($[Na^+]_{stem}$), and roots ($[Na^+]_{root}$) were then determined using a Flame Photometry (PE-pinAAcle, 900 F) according to Ma et al. (2021). Similarly, the K^+ concentration in the leaves ($[K^+]_{leaf}$), stems ($[K^+]_{stem}$), roots ($[K^+]_{root}$) were also determined separately.

2.4.4. Determination of root morphology

After harvesting the above-ground stems and leaves separately, the roots were collected. In detail, the root system was collected by digging out the entire soil column in the pot and retrieving all the roots using tweezers. The roots ware then rinsed in a 2 mm nylon mesh bag and scanned by a root system reader (EPSON Perfection V700, Epson America, Inc.) and analyzed by WinRHIZO Pro software (Version 2012b; Regent Instruments Inc., Québec, QC, Canada) according to Liu et al. (2022b). The root morphological features mainly included root average diameter (RAD, mm), root length (RL, cm), root volume (RV, cm^3), root surface area (RSA, cm^2). Later, the roots were oven dried to constant mass in the oven Then, according to Li et al. (2009), Alhaj Hamoud et al. (2019), and Wang et al. (2021a), the specific root length (SRL, m g^{-1}), specific root volume (SRV, cm^3 g^{-1}), specific root surface area (SRA, cm^2 g^{-1}), root weight density (RWD, mg cm^{-3}), root length density (RLD, cm cm^{-3}), root surface area density (RSAD, cm^2 cm^{-3}), and root tissue density (RTD, g cm^{-3}) were computed based on Eqs. (6), (7), (8), (9), (10), (11), and (12), respectively.

$$SRL = RL/RDM \tag{6}$$

$$SRV = RV/RDM \tag{7}$$

$$SRA = RSA/RDM \tag{8}$$

$$RWD = RDM/V \tag{9}$$

$$RLD = RL/V \tag{10}$$

$$RSAD = RSA/V \tag{11}$$

$$RTD = RDM/RV \tag{12}$$

where, RDM (g) is the root dry mass; V (cm^3) is the volume of the soil column.

2.4.5. Partial factor productivity and water use efficiency

According to Alhaj Hamoud et al. (2019) and Li et al. (2023), the partial factor productivity (PFP, g g^{-1}) of nutrients in the applied fertilizer was calculated according to Eq. (13).

$$PFP = SCY/NI \tag{13}$$

where, SCY (g $plant^{-1}$) is the seed cotton yield; NI (g $soil^{-1}$) is the nutrient input.

Meanwhile, according to Li et al. (2018b), water use efficiency at the whole plant level (WUE_t, g L^{-1}) and seed cotton level (WUE_s, g L^{-1}) were calculated based on Eqs. (14) and (15), respectively.

$$WUE_t = DM/WU \tag{14}$$

$$WUE_s = SCY/WU \tag{15}$$

where, DM (g $plant^{-1}$) is the dry biomass of the whole plant, SCY (g $plant^{-1}$) is seed cotton yield, WU (L $plant^{-1}$) is water consumption of the cotton plant.

2.5. Statistical analysis of data

The three-factor ANOVA was performed by SPSS 22.0 (IBM, Corporation, USA) for salt ([S]), biochar ([B]), irrigation ([IR]) and their interactive effects ([S] × [B] × [IR]). Differences between the means were implemented using Tukey's multiple comparisons at the 5 % significance level. Pearson's correlation between the indicators was performed using Origin Pro 2022 (OriginLab Inc., USA).

3. Results

3.1. Characterization of biochar

Images of the Scanning electron micrographs (SEM) of WSP and SWP are presented in Fig. 1. Biochar SEM images reveal the porous structure of the raw material. This porous structure of biochar allows biochar to have a larger surface area and pore volume, which helps to improve the adsorption capacity of biochar. Moreover, WSP has more micro-size pores compared to SWP.

Furthermore, Fourier-transform infrared (FTIR) was executed for the identification of functional groups on the biochar. FTIR spectra revealed that WSP and SWP have different functional groups (Fig. 2). A large number of absorption bands of WSP and SWP are concentrated at wavenumber <3500 cm^{-1}. The SWP is characterized as nine bands at wave numbers 3437, 2919, 1589, 1394, 1089, 880, 803, 570, and 463 cm^{-1}, respectively. The band at 3437 cm^{-1} can be assigned to the stretching vibration of the O—H (Zhang et al., 2019b); The bands at 2919 cm^{-1} as well as 1589 cm^{-1} are associated with the stretching vibrations of aliphatic C—H and aromatic C═C, respectively (Nguyen et al., 2022); The band at 1394 cm^{-1} should be ascribed to phenolic hydroxyl deformation (Tang et al., 2019; Zhang et al., 2021), COO^- symmetric stretching of deprotonated carboxylic acids (Huang et al., 2018) or C—N stretching (Yang and Jiang, 2014); The band at 1089 cm^{-1} could be ascribed to OH in-plane bending cellulose (Purakayastha et al., 2015), or C—C, C—O, C—O—C (Hasan et al., 2020), silicon oxide (Si—O) (Kataki et al., 2017) stretching vibrations; The bands at 880 cm^{-1} as well as 803 cm^{-1} are ascribed to the bending vibrations of aromatic C—H (Liu et al., 2021a; Moussavi and Khosravi, 2012; Purakayastha et al., 2015); The band at 570 cm^{-1} is ascribed to the P═O bending of dicalcium phosphate or phosphate ions (PO_4^{3-}) (Bekiaris et al., 2016; Soria et al., 2020); The band at 463 cm^{-1} is assigned to the asymmetric deformation vibration of the Si—O bond (Nguyen et al., 2022; Zhu et al., 2018). Similarly, the WSP is characterized as seven bands at wave numbers 3415, 1620, 1427, 1081, 779, 694, and 460 cm^{-1}, respectively. The band at 3415 cm^{-1} can be ascribed to the stretching vibration of the O—H (Wang et al., 2019b); The band at 1620 cm^{-1} can be associated with the stretching vibration of aromatic carbon C═C (Nguyen et al., 2022); The band at 1427 cm^{-1} can be associated with phenolic O—H bending (Purakayastha et al., 2015); The band at 1081 cm^{-1} can be correlated with the deformation of C—O (Nair et al., 2020) or Si—O—Si (Margenot et al., 2016; Nguyen et al., 2022); The band at 779 cm^{-1} can be linked to an asymmetric vibration of Si—O (Kamran et al., 2019; Salam et al., 2020); The band at 694 cm^{-1} can be associated with the stretching vibration of C—H in the aromatic ring (Chan and Wang, 2018; Dai et al., 2022; Sahoo et al., 2020); The band at 460 cm^{-1} can be derived from the bending vibration of Si—O (Nguyen et al., 2022).

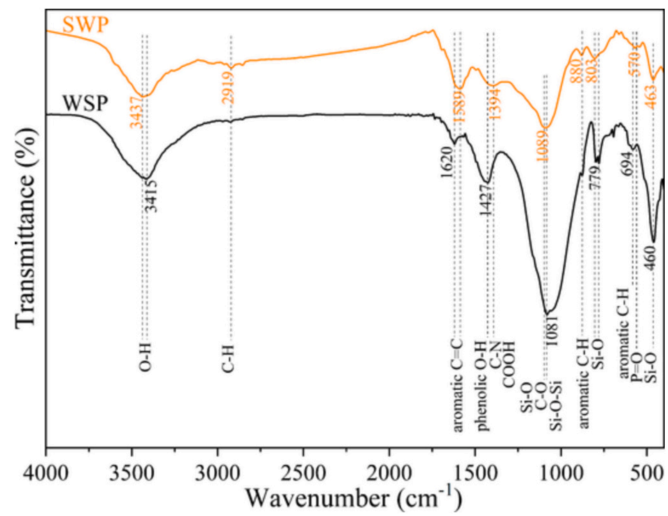

Fig. 2. Fourier-transform infrared (FTIR) spectra of biochar.

3.2. Isothermal adsorption model of biochar on Na^+

To study the adsorption equilibrium of biochar on Na^+, isothermal adsorption experiments were performed. Biochar adsorption of Na^+ (q_e) showed an increase with increasing initial salt concentration (C_i) (Fig. 3). However, there was a slight difference in the adsorption capacity of SWP and WSP for Na^+, with the adsorption of Na^+ by WSP biochar being greater than that by SWP.

On the other hand, the adsorption data were fitted using different isothermal adsorption models, and the fitted parameters of each model are displayed in Table 2. It is evident that the best fit was obtained for the Langmuir model. Moreover, the Langmuir model shows that WSP

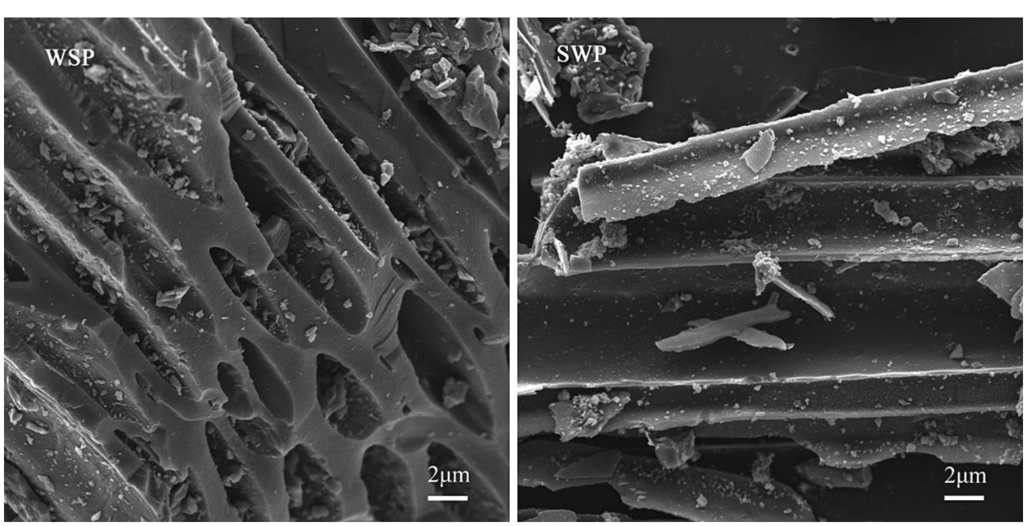

Fig. 1. Scanning electron microscopy (SEM) images of the biochar. (SWP and WSP denote soft wood biochar and wheat straw biochar, respectively. Same below.)

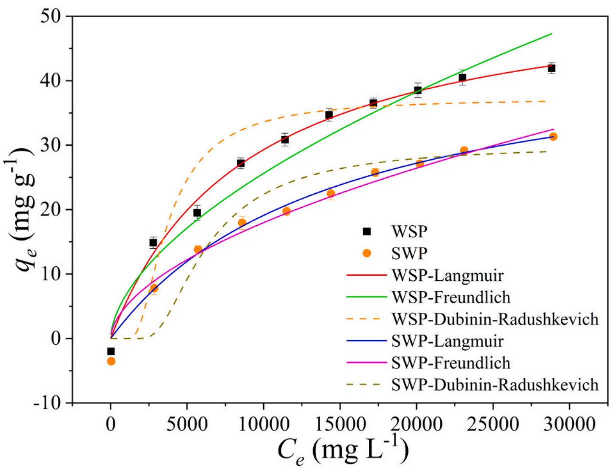

Fig. 3. Isothermal adsorption of Na^+ by WSP and SWP fitted using three isothermal models.

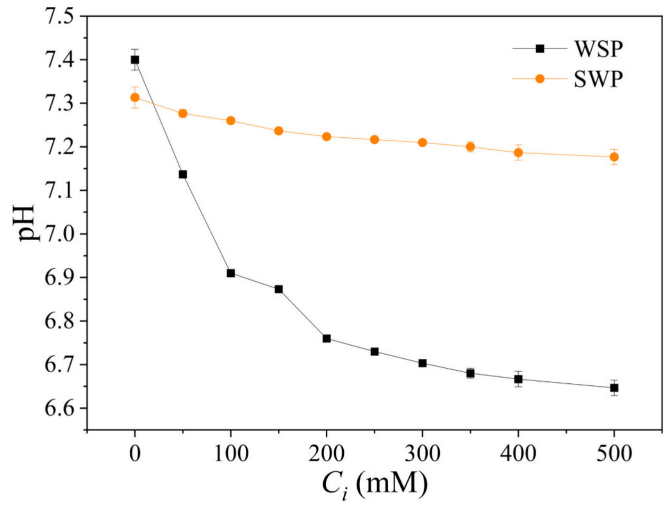

Fig. 4. pH change curves of the equilibrium solutions of WSP and SWP after reaching adsorption equilibrium in different concentrations of salt solutions.

Table 2
Fitting parameters of the adsorption isotherm model for Na^+ adsorption on WSP and SWP.

Isotherm model	Parameters	Biochar	
		WSP	SWP
Langmuir	q_m (mg g^{-1})	55.20 ± 0.88a	47.38 ± 1.91b
	K_l (L mg^{-1})	1.13 × 10^{-4} ± 6.39 × 10^{-6}a	6.95 × 10^{-5} ± 1.07 × 10^{-5}b
	R^2	0.99	0.98
Freundlich	K_f (L g^{-1})	0.44 ± 0.05a	0.12 ± 0.04b
	n	2.22 ± 0.04a	1.82 ± 0.10b
	R^2	0.97	0.97
Dubinin-Radushkevich	q_m (mg g^{-1})	37.53 ± 0.62a	28.55 ± 0.33b
	β (mol^2 KJ^{-2})	1.97 ± 0.35b	4.55 ± 0.62a
	E (kJ mol^{-1})	0.52 ± 0.05a	0.34 ± 0.02b
	R^2	0.75	0.81

has a higher sorption capacity for Na^+ (55.20 mg g^{-1}) compared to SWP (47.38 mg g^{-1}). Dubinin-Radushkevich model shows that the free adsorption energy of WSP is higher than that of SWP, and the free energy of both WSP and SWP is below the threshold of 8 kJ mol^{-1}, suggesting that the process of Na^+ adsorption by WSP and SWP is mainly a physical process.

After the adsorption equilibrium, we determined the pH of the solution in equilibrium. The results suggested that the pH of the equilibrium solution gradually decreased with increasing salt concentration (Fig. 4). The reduction in pH of WSP was greater than that of SWP. The pH value in the equilibrium solution of SWP dropped from 7.31 to 7.18, while the pH value in the equilibrium solution of WSP fell from 7.40 to 6.65.

3.3. *Root morphological characteristics of cotton plants in response to different biochar amendments and irrigation strategies under salt stress*

Analyzing the root characteristics (Table 3), [S] had significant effects on RL, RAD, RSA, RV, SRL, SRA, SRV, RLD, RWD, RTD, RSAD. Salt stress significantly reduced RL, RSA, RV, SRL, RWD, RSAD, SRA, and RLD by 51.03 %–69.13 %, 39.07 %–58.25 %, 19.07 %–46.25 %, 38.30 %–61.02 %, 4.09 %–37.79 %, 39.07 %–58.25 %, 24.97 %–48.95 %, and 51.03 %–69.13 %, respectively. Also, salt stress significantly increased RAD and RTD by 12.49 %–45.16 %, and 0.26 %–78.67 %, respectively. However, biochar amendment significantly increased RL, RSA, RLD, RV, SRL, RWD, RSAD compared to CK. Further, WSP was preferable to SWP in promoting root growth and improving root morphology. The WSP amendment significantly increased RV by 9.52 %–56.14 % in comparison to SWP. DI and PRD allowed enhancing SRL by 0.45 %–47.63 % in comparison to FI. Furthermore, compared to DI, PRD contributed to an increase in RL, RV, RSA, RLD, RWD, and RSAD by 6.50 %–34.44 %, 3.61 %–26.63 %, 6.93 %–30.70 %, 6.50 %–34.44 %, 10.95 %–27.63 %, and 6.93 %–30.70 % respectively.

3.4. *K^+ concentration, Na^+ concentration, and K^+/Na^+ ratio in different organs of cotton plants*

Obviously, [S] and [B] had significant effects on $[Na^+]_{leaf}$, $[Na^+]_{stem}$, $[Na^+]_{root}$, $[K^+]_{leaf}$, $[K^+]_{stem}$, $[K^+]_{root}$, $[K^+/Na^+]_{leaf}$, $[K^+/Na^+]_{stem}$, and $[K^+/Na^+]_{root}$, respectively (Fig. 5, Table 4). Irrespective of [B] and [IR], salt stress made Na^+ concentration rise, lowered K^+ concentration and K^+/Na^+ ratio of different organs. However, biochar amendment resulted in lower Na^+ concentration, higher K^+ concentration and K^+/Na^+ ratio in different organs. Under S1, in comparison to FI, DI and PRD led to elevated $[Na^+]_{leaf}$, $[Na^+]_{stem}$ and $[Na^+]_{root}$ by 13.36 %–54.03 %, 12.12 %–18.66 %, 6.73 %–12.19 %, and 3.53 %–23.66 %, 1.56 %–9.36 %, 2.00 %–3.50 %, respectively. Moreover, PRD reduced $[Na^+]_{leaf}$, $[Na^+]_{stem}$ and $[Na^+]_{root}$ by 7.77 %–19.72 %, 2.46 %–12.58 %, and 3.99 %–9.08 %, respectively, compared to DI. However, under S0, DI and PRD reduced $[Na^+]_{leaf}$, $[Na^+]_{stem}$ by 8.99 %–21.03 %, 17.87 %–34.84 % and 10.65 %–23.66 %, 22.18 %–29.79 % compared to the FI, respectively. Under S1, biochar application led to a significant reduction in $[Na^+]_{leaf}$, $[Na^+]_{stem}$, and $[Na^+]_{root}$ by 10.11 %–33.84 %, −0.62 %-17.54 % and 3.62 %–11.02 %, respectively. Further, compared to the SWP, the WSP amendment significantly reduced $[Na^+]_{leaf}$, $[Na^+]_{stem}$ and $[Na^+]_{root}$ by −7.52 %-16.89 % (except for [S1, WSP, FI] which made $[Na^+]_{leaf}$ increased by 7.52 % compared to [S1, SWP, FI]), 8.56 %–16.56 %, 2.95 %–6.94 % under S1.

In addition, biochar amendment resulted in significantly higher $[K^+]_{leaf}$, $[K^+]_{stem}$, and $[K^+]_{root}$ compared to the CK. In particular, under S1, the biochar amendment resulted in significantly higher $[K^+]_{leaf}$, $[K^+]_{stem}$, and $[K^+]_{root}$ by 2.36 %–83.04 %, 2.01 %–70.67 %, and 7.48 %–33.91 % compared to CK. Furthermore, under S1, the WSP amendment significantly elevated $[K^+]_{leaf}$, $[K^+]_{stem}$, and $[K^+]_{root}$ by 28.17 %–69.13 %, 38.22 %–58.75 %, and 3.05 %–18.79 % (except for [S1, WSP, DI] which made $[K^+]_{root}$ decreased by 8.73 % compared to [S1, SWP, DI]) compared to the SWP. In addition, in general, DI and PRD led to a reduction in $[K^+]_{leaf}$, $[K^+]_{stem}$, and $[K^+]_{root}$ compared to the FI. In particular, under S1, PRD elevated $[K^+]_{leaf}$ by 2.21 %–12.83 % compared to DI.

For the K^+/Na^+ ratios of different organs, salt stress markedly

Table 3
Root morphological characteristics [root length (RL), root volume (RV), root average diameter (RAD), root surface area (RSA), specific root length (SRL), specific root surface area (SRA), specific root volume (SRV), root weight density (RWD), root length density (RLD), root surface area density (RSAD), and root tissue density (RTD)] are affected by different salinity ([S]), different biochar ([B]) and different irrigation regimes ([IR]) in cotton plants and their interaction effects.

Salt	Biochar	Irrigation	RL (cm)	RAD (mm)	RSA (cm^2)	RV (cm^3)	SRL (m g^{-1})	SRA (cm^2 g^{-1})	SRV (cm^3 g^{-1})	RLD (cm cm^{-3})	RWD (mg cm^{-3})	RTD (g cm^{-3})	RSAD (cm^2 cm^{-3})
S0	CK	FI	4654.47 ± 366.40cdef	0.60 ± 0.02bcd	823.83 ± 29.42defg	12.85 ± 0.25cdef	7.70 ± 1.40abc	134.36 ± 18.68abc	2.07 ± 0.22ab	0.31 ± 0.02cdef	0.43 ± 0.05bcd	0.50 ± 0.06ab	0.05 ± 0.00cdef
		DI	5885.51 ± 442.43cd	0.54 ± 0.02cd	905.02 ± 65.11cdef	12.73 ± 0.98cdef	8.69 ± 0.85abc	133.60 ± 12.65abc	1.88 ± 0.18ab	0.39 ± 0.03bcde	0.46 ± 0.01abcd	0.55 ± 0.05ab	0.06 ± 0.00bcdef
		PRD	6372.80 ± 397.69bc	0.58 ± 0.00bcd	1054.84 ± 72.82bcd	15.59 ± 1.25abc	8.61 ± 0.82abc	141.93 ± 12.54abc	2.10 ± 0.20ab	0.42 ± 0.03bcd	0.51 ± 0.05abc	0.49 ± 0.04ab	0.07 ± 0.00abcd
	WSP	FI	6805.10 ± 954.74bc	0.63 ± 0.03abcd	1195.26 ± 130.49bc	19.11 ± 1.49ab	9.71 ± 1.72abc	169.69 ± 24.95ab	2.70 ± 0.30a	0.45 ± 0.06bc	0.48 ± 0.02abcd	0.39 ± 0.05b	0.08 ± 0.01abc
		DI	8584.91 ± 1545.04ab	0.50 ± 0.02d	1315.59 ± 220.54ab	17.91 ± 2.30ab	11.68 ± 2.36a	179.04 ± 34.85a	2.43 ± 0.39ab	0.57 ± 0.10ab	0.50 ± 0.02abc	0.44 ± 0.06b	0.09 ± 0.01abc
		PRD	10,353.81 ± 531.83a	0.49 ± 0.02d	1523.18 ± 118.25a	19.80 ± 2.15a	11.90 ± 0.53a	174.65 ± 9.91ab	2.27 ± 0.21ab	0.69 ± 0.04a	0.58 ± 0.03a	0.45 ± 0.04b	0.10 ± 0.01a
	SWP	FI	5327.10 ± 968.48cde	0.62 ± 0.04abcd	944.93 ± 142.47cde	15.26 ± 1.72abc	8.35 ± 1.73abc	147.50 ± 26.51abc	2.37 ± 0.34ab	0.36 ± 0.06bcdef	0.44 ± 0.02abcd	0.45 ± 0.07b	0.06 ± 0.01bcde
		DI	6416.70 ± 430.90bc	0.54 ± 0.02cd	1037.72 ± 62.11bcd	14.72 ± 0.99bcd	9.34 ± 0.49abc	151.76 ± 10.60abc	2.16 ± 0.19ab	0.43 ± 0.03bcd	0.46 ± 0.03abcd	0.47 ± 0.04ab	0.07 ± 0.00abcd
		PRD	8626.79 ± 1452.98ab	0.53 ± 0.03cd	1356.27 ± 191.81ab	18.64 ± 1.92ab	10.97 ± 1.70ab	173.12 ± 22.27ab	2.39 ± 0.23ab	0.58 ± 0.10ab	0.52 ± 0.04ab	0.43 ± 0.04b	0.09 ± 0.01ab
S1	CK	FI	2078.91 ± 317.70g	0.81 ± 0.03a	501.97 ± 63.15gh	10.40 ± 1.04def	3.84 ± 0.51c	92.81 ± 9.56abc	1.92 ± 0.14ab	0.14 ± 0.02f	0.36 ± 0.03cde	0.53 ± 0.04ab	0.03 ± 0.00ef
		DI	1841.32 ± 130.57g	0.75 ± 0.02ab	411.84 ± 29.68h	8.14 ± 0.84f	4.46 ± 0.52c	100.24 ± 12.61abc	1.99 ± 0.29ab	0.12 ± 0.01f	0.28 ± 0.03e	0.55 ± 0.11ab	0.03 ± 0.00f
		PRD	1967.04 ± 262.79g	0.75 ± 0.02ab	440.39 ± 34.50h	8.44 ± 0.46ef	3.86 ± 0.40c	86.85 ± 5.45bc	1.67 ± 0.11ab	0.13 ± 0.02f	0.34 ± 0.01de	0.61 ± 0.04ab	0.03 ± 0.00ef
	WSP	FI	3039.21 ± 200.82efg	0.71 ± 0.05abc	650.00 ± 47.69efgh	12.81 ± 1.33cdef	4.47 ± 0.30c	95.90 ± 8.00abc	1.89 ± 0.22ab	0.20 ± 0.01def	0.45 ± 0.01abcd	0.55 ± 0.08ab	0.04 ± 0.00def
		DI	3047.78 ± 421.25efg	0.65 ± 0.04abcd	620.07 ± 58.29efgh	11.26 ± 0.79cdef	5.38 ± 0.52bc	110.05 ± 5.55abc	2.01 ± 0.09ab	0.20 ± 0.03def	0.37 ± 0.02bcde	0.50 ± 0.02ab	0.04 ± 0.00def
		PRD	3245.89 ± 290.08efg	0.71 ± 0.02abc	669.76 ± 50.85efgh	12.95 ± 1.01cde	4.64 ± 0.65c	95.68 ± 12.64abc	1.85 ± 0.26ab	0.22 ± 0.02def	0.48 ± 0.03abcd	0.57 ± 0.07ab	0.04 ± 0.00def
	SWP	FI	2363.13 ± 718.58fg	0.74 ± 0.10ab	459.67 ± 99.04h	8.20 ± 1.01ef	3.90 ± 1.29c	75.30 ± 18.49c	1.33 ± 0.21c	0.16 ± 0.05ef	0.42 ± 0.03bcde	0.81 ± 0.12a	0.03 ± 0.01ef
		DI	3142.31 ± 673.03efg	0.67 ± 0.03abcd	599.75 ± 92.18fgh	10.28 ± 1.12def	5.76 ± 1.39bc	110.26 ± 22.79abc	1.90 ± 0.36ab	0.21 ± 0.04def	0.38 ± 0.04bcde	0.58 ± 0.10ab	0.04 ± 0.01def
		PRD	3732.70 ± 837.15defg	0.65 ± 0.03abcd	691.04 ± 117.76efgh	11.72 ± 1.50cdef	5.48 ± 1.32bc	101.28 ± 18.55abc	1.71 ± 0.23ab	0.25 ± 0.06cdef	0.46 ± 0.01abcd	0.62 ± 0.08ab	0.05 ± 0.01def
ANOVA factor													
Salt ([S])			***	***	***	***	***	***	***	***	***	***	***
Biochar ([B])			***	*	***	***	*	ns	ns	***	***	ns	***
Irrigation ([IR])			***	***	**	*	ns	ns	ns	***	***	ns	**
[S] × [B]			ns	ns	ns	ns	ns	ns	ns	ns	ns	ns	ns
[S] × [IR]			*	ns	ns	ns	ns	ns	ns	*	*	ns	ns
[B] × [IR]			ns	ns	ns	ns	ns	ns	ns	ns	ns	ns	ns
[S] × [B] × [IR]			ns	ns	ns	ns	ns	ns	ns	ns	ns	ns	ns

Notes: ***, **, * represents significant at P < 0.001, P < 0.01, P < 0.05 level, respectively, 'ns' represents no significance.

lowered $[K^+/Na^+]_{leaf}$, $[K^+/Na^+]_{stem}$, and $[K^+/Na^+]_{root}$ by 49.49 %–79.17 %, 46.18 %–74.05 %, and 30.17 %–66.82 %. However, biochar addition alleviated the reduction of $[K^+/Na^+]$ in different organs of cotton plants. Moreover, the WSP amendment elevated $[K^+/Na^+]$ to a greater extent compared to the SWP amendment. In detail, compared to CK, WSP significantly elevated $[K^+/Na^+]_{leaf}$, $[K^+/Na^+]_{stem}$, and $[K^+/Na^+]_{root}$ by 48.97 %–141.27 %, 25.40 %–99.76 %, and 31.64 %–119.10 %, respectively, yet SWP significantly elevated $[K^+/Na^+]_{leaf}$, $[K^+/Na^+]_{stem}$, and $[K^+/Na^+]_{root}$ by only 14.91 %–85.80 %, 7.23 %–61.15 %, and 9.37 %–39.07 %, respectively. There was a significant interaction of [S] × [IR] on $[K^+/Na^+]_{leaf}$ (Table 4). Under S1, DI and PRD made the $[K^+/Na^+]_{leaf}$ decrease by 25.27 %–55.49 % and 9.87 %–43.13 % compared to FI, respectively. Moreover, under S0 and S1, PRD treatment elevated $[K^+/Na^+]_{leaf}$ by 3.24 %–27.77 % compared to DI (Fig. 6).

3.5. Water use efficiency and partial factor productivity of nutrients of cotton plants in response to different biochar amendments and irrigation strategies under salt stress

Salt stress remarkably declined the dry biomass (DM) and the partial factor (N, P, and K) productivity of nutrients in comparison to the S0, but significantly raised the WUE_t and WUE_s (Table 5; Fig. S2). In detail, the DM and the partial factor (N, P, and K) productivity was significantly reduced by 27.41 %–47.52 % and 17.81 %–47.22 % under S1 compared to S0, but WUE_t and WUE_s were significantly increased by 2.65 %–34.88 % and 3.25 %–61.26 %. Furthermore, under S0, the biochar amendment resulted in a significant elevation of DM and PFP by 5.78 %–13.36 % and 7.02 %–16.83 %, respectively, although it slightly reduced the WUE_t and WUE_s by 2.44 %–5.60 % and 0.23 %–6.51 %. Under S1, the biochar application not only led to a significant elevation in the PFP and DM, but also in WUE_t and WUE_s. Further, the WSP amendment significantly increased the PFP compared to SWP. In addition, the WSP significantly boosted WUE_t and WUE_s under S1. Also, the DI and PRD significantly

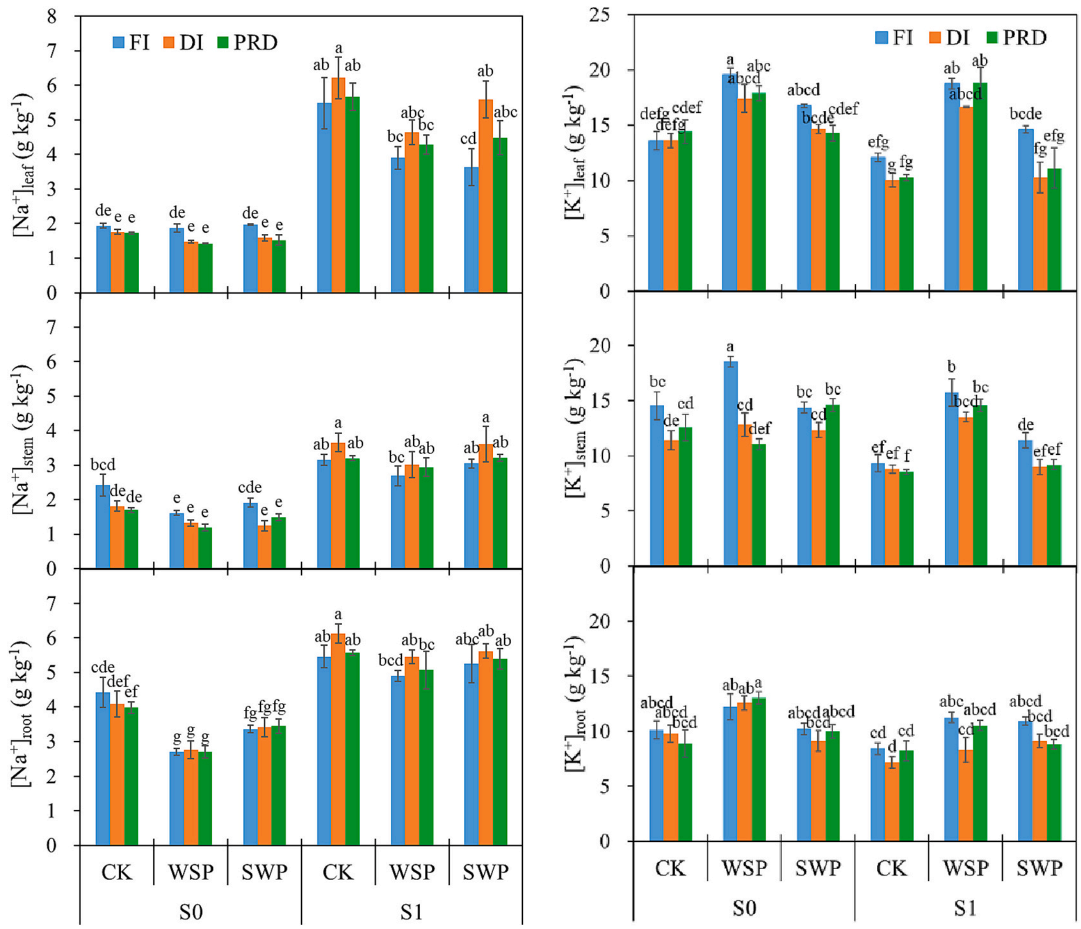

Fig. 5. Sodium concentration in leaves ($[Na^+]_{leaf}$), stems ($[Na^+]_{stem}$), roots ($[Na^+]_{root}$), potassium concentration in leaves ($[K^+]_{leaf}$), stems ($[K^+]_{stem}$), roots ($[K^+]_{root}$) of cotton plants exposed to different salinity levels (S0 and S1), different biochar amendments (CK, no biochar amendment; WSP, wheat straw biochar amendment; SWP, soft wood biochar amendment) and different irrigation strategies (DI, deficit irrigation; PRD, partial root-zone drying irrigation; FI, full irrigation). The three-factor ANOVA for salinity, biochar, irrigation, and their interaction effects are exhibited in Table 4. The values displayed in the graph are means ± standard error (n = 4), same as below.

Table 4
Output of three-factor ANOVA for sodium concentration in leaves ($[Na^+]_{leaf}$), stems ($[Na^+]_{stem}$), roots ($[Na^+]_{root}$), potassium concentration in leaves ($[K^+]_{leaf}$), stems ($[K^+]_{stem}$), roots ($[K^+]_{root}$), ratio of potassium concentration to sodium concentration in leaves ($[K^+/Na^+]_{leaf}$), stems ($[K^+/Na^+]_{stem}$), roots ($[K^+/Na^+]_{root}$), and dry biomass (DM) of cotton plants as affected by salt ([S]), biochar ([B]), and irrigation ([IR]) and their interactive effects.

ANOVA factor	$[Na^+]_{leaf}$ (g kg^{-1})	$[Na^+]_{stem}$ (g kg^{-1})	$[Na^+]_{root}$ (g kg^{-1})	$[K^+]_{leaf}$ (g kg^{-1})	$[K^+]_{stem}$ (g kg^{-1})	$[K^+]_{root}$ (g kg^{-1})	$[K^+/Na^+]_{leaf}$ (g kg^{-1})	$[K^+/Na^+]_{stem}$ (g kg^{-1})	$[K^+/Na^+]_{root}$ (g kg^{-1})	DM (g plant^{-1})
Salt ([S])	***	***	***	***	***	***	***	***	***	***
Biochar ([B])	***	***	***	***	***	***	***	***	***	***
Irrigation ([IR])	ns	*	ns	***	ns	***	ns	ns	ns	***
[S]×[B]	ns	*	*	**	**	***	*	**	***	*
[S]×[IR]	***	ns	ns	ns	**	ns	***	ns	ns	*
[B]×[IR]	ns	ns	ns	ns	ns	*	ns	*	ns	ns
[S]×[B]×[IR]	ns	ns	ns	ns	ns	**	ns	*	ns	ns

Notes: ***, **, * represents significant at P < 0.001, P < 0.01, P < 0.05 level, respectively, 'ns' represents no significance. The data are presented in Fig. 5, Fig. 6 and Fig. S2.

reduced the PFP in comparison to the FI. However, in comparison to DI, PRD significantly increased the PFP by 9.71 %–24.51 %. PRD also significantly improved WUE_t and WUE_s in comparison to DI.

3.6. The correlation between the different indicators

As shown in Fig. 7, correlation coefficient analysis showed that PFP and DM had significant positive correlations with $[K^+]_{root}$, $[K^+]_{stem}$, and $[K^+]_{leaf}$. RL, RSA, RV, RWD, RSAD, and DM had negative correlations with $[Na^+]_{root}$, $[Na^+]_{stem}$, and $[Na^+]_{leaf}$. Furthermore, $[K^+/Na^+]_{root}$, $[K^+/Na^+]_{stem}$, and $[K^+/Na^+]_{leaf}$ had significant positive correlations with RL, RSA, RV, SRL, SRA, RLD, RWD, RSAD, and DM, respectively, and negative correlations with RAD.

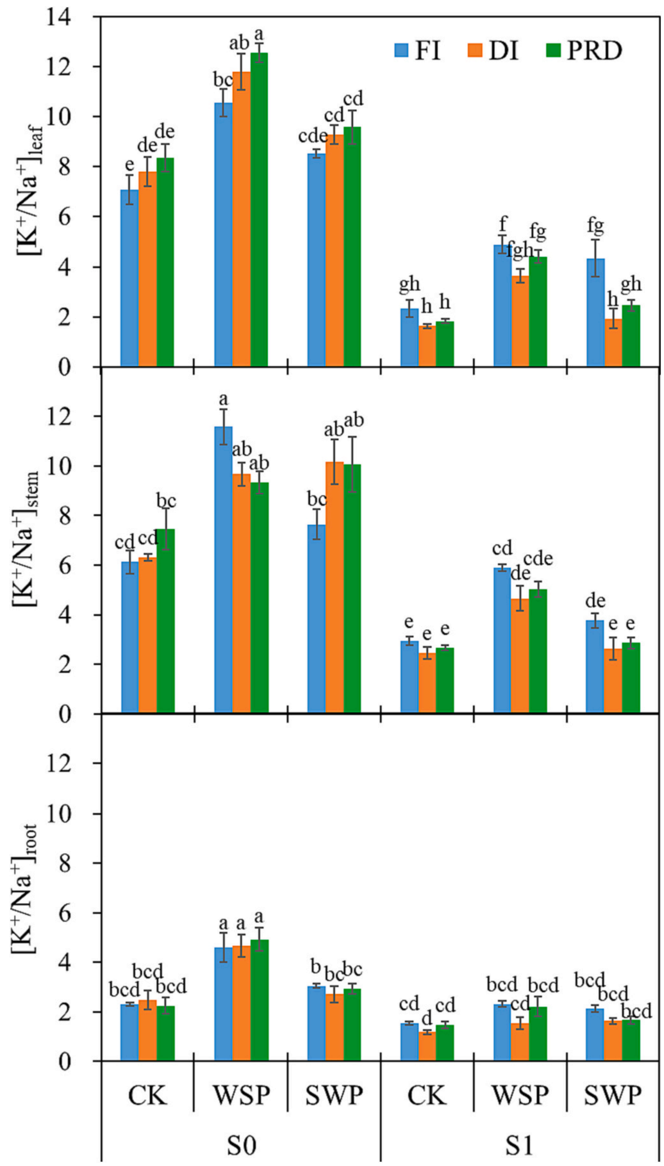

Fig. 6. Ratio of potassium concentration to sodium concentration in leaves ($[K^+/Na^+]_{leaf}$), stems ($[K^+/Na^+]_{stem}$), roots ($[K^+/Na^+]_{root}$) of cotton plants exposed to different salinity levels (S0 and S1), different biochar amendments (CK, no biochar amendment; WSP, wheat straw biochar amendment; SWP, soft wood biochar amendment) and different irrigation strategies (DI, deficit irrigation; PRD, partial root-zone drying irrigation; FI, full irrigation). The three-factor ANOVA for salinity, biochar, irrigation, and their interaction effects are exhibited in Table 4.

4. Discussion

To reveal the mechanisms by which biochar combined with partial root-zone drying irrigation alleviate salinity and drought stress in cotton plants, root morphology, potassium and sodium uptake, water use efficiency and partial factor productivity were analyzed. Apart from that, different isothermal adsorption models were used to elucidate the adsorption behavior of the biochars on Na^+ in order to partly explain the reasons of biochar addition on alleviating salt stress in cotton plants.

4.1. Adsorption behavior of biochar on sodium ions

From the FTIR spectra (Fig. 2), it can be seen that SWP and WSP have significantly broad and intense absorption peaks at 3437 cm^{-1} as well as 3415 cm^{-1}, respectively, which are mainly ascribed to the stretching vibration of hydroxyl (O—H) (Wang et al., 2019b; Zhang et al., 2019b). This also indicates that the biochar surface has a large number of O—H, and the H^+ in the O—H functional groups provides adsorption sites for ion exchange with Na^+ (Cai et al., 2022). Besides, we found that, compared to other models, Langmuir model fitted the best for the isothermal adsorption capacity of different biochar for Na^+, consistent with the findings by Nguyen et al. (2022). This also suggests that the monolayer adsorption of Na^+ occurs on an energy-equivalent homogeneous site on the surface of the biochar. Furthermore, based on the Langmuir isotherm model, the maximal adsorption capacities for WSP and SWP were found to be 55.20 mg g^{-1} and 47.38 mg g^{-1}, respectively, both of which were greater than the maximal adsorption capacity of 33.9 mg g^{-1} for Na^+ reported by Nguyen et al. (2022). This may be related to the raw material of the biochar and the different pyrolysis temperatures. The biochar used in Nguyen et al. (2022) was obtained at a pyrolysis temperature of 350 °C, while the biochar we used was produced at 550 °C. This allowed the biochar used in our experiments to have a larger BET surface area, thus increasing the adsorption capacity for Na^+. Similarly, Rostamian et al. (2018) suggested that the adsorption capacity of biochar for Na^+ ranged from 35.2 to 60.8 mg g^{-1}. And, Akhtar et al. (2015a) showed that biochar made from a blend of softwood and hardwood can have an adsorption capacity for Na^+ higher than 60 mg g^{-1}. However, Awan et al. (2020) showed that biochar made from hemp had an adsorption capacity of 0.923 mg g^{-1} for Na^+. It is thus clear that both the raw material of biochar and the pyrolysis temperature could affect the adsorption capacity. Besides, Dubinin-Radushkevich model is usually suitable for inhomogeneous surfaces of adsorbents (Malik et al., 2017) and can also be used to evaluate the Gibbs free energy (Liu et al., 2022a; Srivastava et al., 2015). In our experiments, the fitting of the Dubinin-Radushkevich model suggests that the free energy for Na^+ adsorption is below 8 KJ mol^{-1}, implying that the adsorption process of biochar for Na^+ is primarily a physical process (Taha et al., 2016). This physical process may involve electrostatic forces, van der Waals forces, hydrogen bonding, hydrophobic interactions (Awan et al., 2020; Zhang et al., 2016).

In addition, in the present study we found that WSP had a higher sorption capacity than SWP, indicating that biochar produced from herbaceous species possesses a higher adsorption capacity for Na^+ than biochar produced from soft wood. This may be due to the fact that wood-derived biochar possesses a higher lignin content (Qiu et al., 2022), which limits the development of pores (Soria et al., 2020). This can also be reflected from the fact that WSP has a larger total pore volume compared to SWP, in agreement with Kozyatnyk et al. (2021). Also, Trakal et al. (2014) showed that wood-derived biochar with high lignin content had less adsorption capacity than herbaceous-derived biochar. In addition to this, the pH value of biochar may also be a factor influencing the adsorption performance. The pH value is an essential feature that affects the biochar quality, and a higher pH value suggests a higher carbonization degree (Ahmed and Hameed, 2020). In this study, the WSP has a higher pH than SWP (Table 1), which would allow the oxygen-containing functional groups of WSP to have more negative charges during deprotonation and thus can adsorb more Na^+ than SWP (Pahlavan et al., 2023). In addition, the FTIR spectra results revealed that WSP has a more intense absorption peak at 1081 cm^{-1} than SWP, which could be mainly attributed to the bending vibrations of oxygen-containing groups like C—O, Si—O, and Si—O—Si (Margenot et al., 2016; Nair et al., 2020; Nguyen et al., 2022). This would have contributed to the higher adsorption capacity of WSP compared to SWP. In fact, previous reports have pointed out that oxygen-containing functional groups on the surface of biochar can adsorb cations from the surrounding environment through various mechanisms (Ahmad et al., 2014; Guo et al., 2020; Mireles et al., 2019; Nguyen et al., 2022).

According to Palomino and Santamarina (2005), to quantify ionic exchange of biochar with solution, the solution pH after the adsorption equilibrium needs to be measured. Here we found that the pH of the equilibrium solution gradually drops as the salt concentration in the

Table 5
Water use efficiency at the whole plant level (WUE_t) and seed cotton level (WUE_s) and partial factor productivity of nutrients (PFP) under the influence of salinity ([S]), biochar ([B]), irrigation ([IR]), and their interaction effects.

Salt	Biochar	Irrigation	WUE_t ($g\ L^{-1}$)	WUE_s ($g\ L^{-1}$)	PFP ($g\ g^{-1}$)		
					N	P	K
S0	CK	FI	2.17 ± 0.07de	0.43 ± 0.01e	13.12 ± 0.32abc	24.22 ± 0.58abc	19.22 ± 0.46abc
		DI	2.18 ± 0.08de	0.45 ± 0.02e	10.49 ± 0.49de	19.37 ± 0.91de	15.37 ± 0.72de
		PRD	2.36 ± 0.06cde	0.49 ± 0.03de	11.51 ± 0.82cd	21.25 ± 1.51cd	16.86 ± 1.20cd
	WSP	FI	2.05 ± 0.04e	0.42 ± 0.00e	15.03 ± 0.37a	27.74 ± 0.68a	22.01 ± 0.54a
		DI	2.11 ± 0.07e	0.43 ± 0.01e	11.63 ± 0.18cd	21.47 ± 0.34cd	17.03 ± 0.27cd
		PRD	2.26 ± 0.03cde	0.48 ± 0.00de	13.45 ± 0.16abc	24.82 ± 0.29abc	19.70 ± 0.23abc
	SWP	FI	2.12 ± 0.15e	0.42 ± 0.01e	14.28 ± 0.69ab	26.35 ± 1.27ab	20.91 ± 1.01ab
		DI	2.11 ± 0.07e	0.42 ± 0.02e	11.23 ± 0.62cd	20.73 ± 1.14cd	16.45 ± 0.91cd
		PRD	2.27 ± 0.04cde	0.49 ± 0.01de	12.61 ± 0.40bcd	23.26 ± 0.73bcd	18.46 ± 0.58bcd
S1	CK	FI	2.44 ± 0.07bcde	0.57 ± 0.02cd	8.47 ± 0.59ef	15.63 ± 1.09ef	12.41 ± 0.87ef
		DI	2.24 ± 0.07cde	0.47 ± 0.02e	5.54 ± 0.29g	10.22 ± 0.53g	8.11 ± 0.42g
		PRD	2.55 ± 0.11abcd	0.57 ± 0.03cd	6.78 ± 0.39fg	12.51 ± 0.72fg	9.93 ± 0.57fg
	WSP	FI	2.76 ± 0.08ab	0.68 ± 0.02ab	12.12 ± 0.20bcd	22.37 ± 0.38bcd	17.75 ± 0.30bcd
		DI	2.59 ± 0.10abc	0.62 ± 0.01bc	8.61 ± 0.22ef	15.89 ± 0.41ef	12.61 ± 0.32ef
		PRD	2.89 ± 0.09a	0.74 ± 0.02a	10.72 ± 0.33de	19.79 ± 0.61de	15.70 ± 0.48de
	SWP	FI	2.43 ± 0.04bcde	0.61 ± 0.02bc	11.32 ± 0.47cd	20.89 ± 0.87cd	16.57 ± 0.69cd
		DI	2.54 ± 0.08abcd	0.59 ± 0.04c	8.43 ± 0.55ef	15.56 ± 1.02ef	12.35 ± 0.81ef
		PRD	2.89 ± 0.06a	0.71 ± 0.02a	10.36 ± 0.31de	19.12 ± 0.57de	15.17 ± 0.45de
ANOVA factor							
Salt ([S])			***	***	***	***	***
Biochar ([B])			*	***	***	***	***
Irrigation ([IR])			***	***	***	***	***
[S] × [B]			***	***	***	***	***
[S] × [IR]			ns	**	ns	ns	ns
[B] × [IR]			ns	ns	ns	ns	ns
[S] × [B] × [IR]			ns	ns	ns	ns	ns

Notes: ***, **, * represents significant at P < 0.001, P < 0.01, P < 0.05 level, respectively, 'ns' represents no significance.

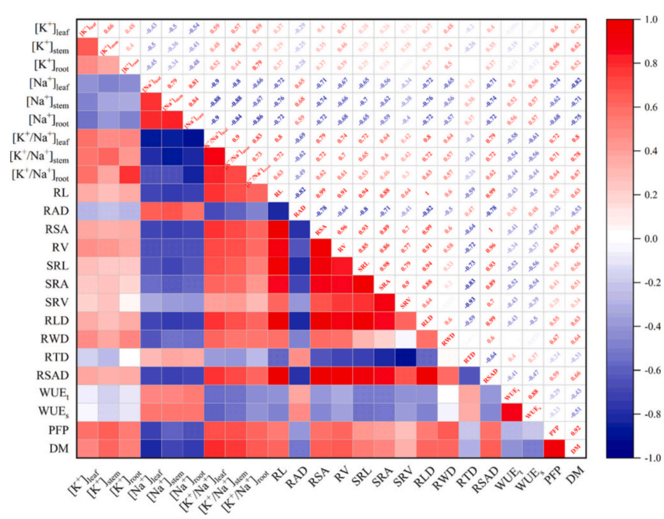

Fig. 7. Correlation plots between sodium ion concentration, potassium ion concentration in different organs, root morphological characteristics and water use efficiency and partial factor productivity.

initial solution increases, which is consistent with Cai et al. (2022). This is mainly because of the exchangeable H^+ in the functional groups being exchanged into the solution by Na^+ (Cai et al., 2022), indicating that biochar can adhere Na^+ via hydrophilic functional groups like -OH and -COOH, and promote the precipitation of salts (Moradi et al., 2019; Rajapaksha et al., 2016). Moreover, the greater decrease in pH of the equilibrium solution of WSP compared to SWP suggests that more exchangeable H^+ on the surface of WSP was replaced by Na^+, which also implies that WSP has greater adsorption of Na^+ compared to SWP. The Langmuir coefficient K_l for WSP was greater than for SWP also indicates WSP has a stronger capacity for Na^+ adsorption than SWP.

4.2. Response of root morphological characteristics of cotton plants to biochar application and irrigation strategy under salt stress

In line with earlier reports (Chen et al., 2018; Dai et al., 2014; Liu et al., 2020; Ren et al., 2022), our experiment showed that salt stress caused a significant decrease of RL, RSA, RV, SRL, SRA, RLD, RWD, RSAD in cotton plants. Also, salt stress caused an increase in RAD, which is consistent with previous literature (Chen et al., 2020; Li et al., 2023; Min et al., 2014). The increase of RAD may be attributed to the fact that salinity reduces the percentage of fine roots (Chen et al., 2020) and makes the root cortex succulent (Casenave et al., 1999; Rewald et al., 2012). On the other hand, our experiments indicated that the DI and PRD strategies increased the RL and decreased the RAD of cotton plants, resulting in a greater RLD, coinciding with earlier reports (Kashiwagi et al., 2006; Siddiqui et al., 2021; Xiao et al., 2020). This may be owed to the fact that soil water deficits caused by DI or PRD stimulated root lengthening and facilitates the formation of more fine roots, but the new fine roots tend to be smaller in diameter and often have longer root hairs (Xiao et al., 2020). Correlation analysis also revealed that RAD was significantly and negatively linked to RL (Fig. 7), in line with the findings by Awad et al. (2018). Additionally, we found significant greater RL, RV, RSA, RLD, RWD, and RSAD of cotton plants under PRD compared to DI, suggesting that the PRD strategy effectively improved root growth in cotton plants, in good agreement with prior reports (Shu et al., 2020; Siddiqui et al., 2021; Wang et al., 2019a; Zhang et al., 2014).

In accordance with earlier reports (Dong et al., 2022; Li et al., 2021; Parkash and Singh, 2020), our experiment showed that biochar amendment led to an increase in RL, RSA, RV and a decrease in RAD. This suggests that biochar amendment has a tendency to make the root system thin and long (Ostonen et al., 2007). This is probably due to that biochar consists of organic compounds such as hydroxyl, alkanoic acid, benzoic acid, phenols, polyols and ethoxylic acids, which can encourage the elongation of roots (Graber et al., 2010; Li et al., 2021). Moreover, biochar can change the mechanistic composition of the soil and reduce the soil mechanical resistance, thus contributing to the elongation of fine roots, thus directly or indirectly facilitating root development (Backer et al., 2017; Cheng et al., 2018; Spokas et al., 2011). Further, we found that WSP resulted in greater RL, RSA, RV, SRL, SRA, SRV, RLD, RWD, RSAD compared to SWP. This could be attributed to that WSP possesses a large number of hydrophilic functional groups on its surface due to the richness of cellulose (Jing et al., 2022), which helps to raise the water absorption and the shrinkage limit of the soil, leading to an increased interlayer space in the soil (Cai et al., 2022; Yang et al., 2021) facilitating the elongation of the root system. Besides, we found a negative correlation between RAD and $[K^+]_{root}$, suggesting that plant access to nutrients is strongly influenced by the diameter of the roots (through given length of root or area), as thicker root systems tend to pay the price of lower nutrient uptake rates (Rewald et al., 2013).

4.3. Effect of biochar application and different irrigation strategies on Na^+, K^+ concentration, and K^+/Na^+ ratio in different organs under salt stress

Our experiments showed that salt stress led to an elevated Na^+ concentration and a lowered in K^+ concentration, and decreased K^+/Na^+ ratio cotton plants, in agreement with earlier research (Essa, 2002; Ju et al., 2023). Such effect of slat stress is mainly attributed to the down-regulated expression of potassium ion transporters (e.g., HAK, KT, NHX and HKT), preventing root K^+ uptake, causing a reduction in the intracellular K^+ concentration (Ju et al., 2023).

On the other hand, in agreement with Alvarez and Sanchez-Blanco (2015), our results showed that DI and PRD treatments reduced the Na^+ concentration in leaves, roots, and stems under S0 compared to FI treatment. This may be ascribed to the fact that a low water content of the soil reduces the diffusion of Na^+ to the surface of the roots (Raynaud and Leadley, 2004), resulting in a decrease in Na^+ uptake, and a decrease in Na^+ transport to the shoot due to the reduced transpiration rate caused by drought stress (Munns and Tester, 2008; Pardo, 2010). However, our experiments also showed that DI and PRD treatments caused an elevation in Na^+ concentration in cotton plants under S1. This could be attributed to the fact that reduced irrigation regimes combined with salinity stress caused a greater reduction in plant growth (Alvarez and Sanchez-Blanco, 2015), resulting in a concentration effect of Na^+ in plant organs. Similarly, the study by Alvarez and Sanchez-Blanco (2015) on *Callistemon laevis* showed that the combination of salt stress and drought stress led to a remarkable elevation in Na^+ concentration in roots, stems, and leaves in comparison to the individual effects of drought stress or salt stress. It is noteworthy that the Na^+ concentration of leaves, stalks, and roots under PRD was significantly lower compared to DI. This may be due to the heterogeneous distribution of salt concentration in the soil caused by the PRD strategy (Kong et al., 2017), which induced salt overly sensitive (*SOS*) genes to express (Kong et al., 2012, 2016) and increased the Na^+ efflux capacity (Chen et al., 2017; Qiu et al., 2002; Zhang and Shi, 2013; Zhang et al., 2017), thus reducing Na^+ accumulation in leaves, stalks and roots. Furthermore, Wang et al. (2012) showed that PRD resulted in a reduction in Na^+ concentration within the xylem sap compared to DI. This also suggests that the PRD strategy can improve the salt endurance of plants compared to the DI strategy (Alves et al., 2018; Dong et al., 2010; Hou et al., 2023; Kong et al., 2012, 2016). Likewise, earlier reports on cotton (Dong et al., 2010), tomato (Koushafar et al., 2011; Mulholland et al., 2015), sour orange (Zekri and Parsons, 1990), cucumber (Sonneveld and de Kreij, 1999), alfalfa (Sun et al., 2016; Xiong et al., 2018), *Atriplex nummularia* (Bazihizina et al., 2009), and *Lycium chinense* (Feng et al., 2017) have shown that heterogeneous salt distribution can mitigate the destruction caused to the plant by salt stress compared to homogeneous salt distribution.

In addition, our experiments revealed that K^+ concentrations in roots, stems and leaves of plants under DI and PRD treatments was significantly reduced compared to FI, suggesting that soil water deficits lead to reduced K^+ intake by plants (Hu and Schmidhalter, 2005). This could be caused by the reduced K^+ mobility in the soil due to soil water deficits, reduced transpiration rates of plants, and reduced root membrane transporter activity (Hu et al., 2013; Hu and Schmidhalter, 2005; Shabala and Pottosin, 2014). Despite this, we also found a remarkable elevation in K^+ concentration in different organs under PRD compared to DI, which is coherent with the prior publications (Yang et al., 2020). This could be ascribed to the heterogeneous distribution of salt concentration in the soil compartments caused by PRD, which in turn reduced K^+ loss in the root system as well as improved salt tolerance (Guo et al., 2015; Lai et al., 2014).

It is notable that the PRD strategy resulted in elevated K^+/Na^+ in different organs of the cotton plants compared to the DI. This suggests that the PRD strategy help to sustain the ionic homeostasis in cotton plants. This may be due to the fact that the PRD strategy increased the level of IAA compared to the DI strategy (Kong et al., 2016; Zhang et al., 2019a), which further up-regulated the K^+ transporter gene (e.g. *KAT1/KAT2*) expression (Philippar et al., 2004), increased K^+ aggregation (Xiong et al., 2020), and reduced Na^+ aggregation caused by the recycling of Na^+ regulated by AtHKT1(Berthomieu et al., 2003; Kong et al., 2012), thus maintaining K^+/Na^+ stability (Che et al., 2022). Besides, biochar application enhanced soil K^+ content (Li et al., 2018a; Marks et al., 2016; Oram et al., 2014), which could lead to an up-regulated potassium ion transporters including HAK, KT, NHX and HKT (Ju et al., 2023), facilitating Na^+ efflux and allowing the roots to selectively uptake more K^+ (Horie et al., 2009; Ju et al., 2023).

4.4. Effects of biochar application and irrigation strategy on partial factor productivity of nutrients and water use efficiency of cotton plants

The partial factor productivity (PFP) of nutrients as a composite measure of nutrient use quantifies the yield output relative to all nutrient use (Li et al., 2018a). Our study indicated that biochar application caused a remarkable elevation in DM and PFP of N, P and K, irrespective of salinity stress, in agreement with the previous studies (Li et al., 2018a; Liu et al., 2021b). This may be due to the large amount of nutrients brought into the soil by the biochar application and the improved soil moisture status (Li et al., 2018a). Furthermore, the biochar addition lowered the soil bulk and enhanced the soil permeability, which favors microbial health and root growth (Li et al., 2018a). This is also as we found that RLD has a positive correlation with DM and PFP, respectively, which is consistent with Liao et al. (2022). Moreover, we found that RV, RL, RSA, RWD had a significant positive correlation with PFP, respectively, which is also consistent with Ma et al. (2022). This is also as Sun et al. (2022) suggest that increased cotton yield is closely related to increased root growth. This is because the biochar amendment alleviated salt stress in the rhizosphere microbiota (Zheng et al., 2022) and promoted nutrient uptake (Feng et al., 2021), leading to an increase in root length, root dry mass, and root surface area (Sun et al., 2022), which in turn increased yield and PFP.

In addition, our trials indicated that biochar addition caused a slight downward trend in WUE_t and WUE_s, which is inconsistent with Li et al. (2018a) who showed that biochar application resulted in an increase in WUE_s. Similarly, Liu et al. (2021b) also found that biochar application caused a reduction in WUE_t. Therefore, the response of WUE to biochar addition was dependent on biochar type and soil type (Aller et al., 2017; Gray et al., 2014). In general, WUE tends to decrease under clay or clay loam soils, while it tends to increase or remain unchanged under sandy or sandy loam soils (Aller et al., 2017). This may of course also be linked to the properties of the biochar itself, as the different types of biochar affect the pore structure and thus the water uptake by the biochar, which in turn affects the WUE (Gray et al., 2014). However, although biochar caused a downward trend in WUE_t and WUE_s under S0, biochar amendment caused both WUE_t and WUE_s to increase under S1, which is consistent with Thomas et al. (2013). This also indicates that biochar has a favorable effect on mitigating salinity stress for plant growth.

Moreover, PRD combined with biochar also resulted in an increase in WUE_t, WUE_s, and PFP both in the presence and absence of salinity stress. This was mainly related to the fact that the PRD strategy induced more ABA production in the root system, which in turn led to a reduction in stomatal opening and a significant increase in WUE (Liu et al., 2021c). Of course, PRD-induced 'birch effect' can accelerate soil N mineralization and increase effective N use (Jarvis et al., 2007), contributing to yield, WUE_s and PFP (Liu et al., 2021c; Wang et al., 2018). Also, as discussed in Section 4.3, the PRD strategy increased $[K^+]_{leaf}$ and improved K^+/Na^+ in the plant, thus alleviating salt damage to the plant and allowing for increased yields, which in turn increased PFP, and as we found PFP had a significant positive correlation with $[K^+/Na^+]_{root}$, $[K^+/Na^+]_{stem}$, $[K^+/Na^+]_{leaf}$ (Fig. 7). This is because a higher K^+/Na^+ allows the toxic effects of Na^+ to be minimized (Yue et al., 2012) and is essential for the maintenance of normal cellular function (Chinnusamy et al., 2005).

On the other hand, we found that WSP was always preferable to SWP in boosting WUE_t, WUE_s, DM, and PFP under salt stress. This is not only due to the fact that WSP can adsorb more Na^+ compared to SWP as we discussed in Section 4.1, but also related to the fact that WSP has a smaller C/N ratio compared to SWP. This is because, as Nguyen et al. (2017) reported, higher C/N is more likely to lead to nitrogen immobilization in the soil, thus affecting plant uptake of nitrogen and negatively affecting plant development (Li et al., 2015; Sun et al., 2018). It is also because of the relatively high C/N ratio of SWP that indirectly reduces the WUE_t, WUE_s, and PFP compared to WSP.

5. Conclusions

Salt stress had a detrimental effect on the root morphology of cotton plants, and it caused an increase in Na^+ concentration and a decrease in K^+ concentration and K^+/Na^+ in different organs of the plant. However, the biochar amendment effectively alleviated salt stress, decreased Na^+ concentration, increased K^+ concentration and K^+/Na^+ in the plant, improved root morphology, and raised root length, root surface area, root volume, root weight density, root length density, root surface area density, and dry biomass. The adsorption isotherms of WSP and SWP for Na^+ were in accordance with the Langmuir model, and WSP had a stronger adsorption capacity for Na^+ than SWP. Therefore, under salt stress, WSP amendment had a superior effect in reducing Na^+ uptake, improving root morphology, and increasing dry biomass and partial factor productivity compared to SWP. In addition, PRD was superior to DI in increasing water use efficiency and partial factor productivity. Collectively, the combined application of WSP and PRD can effectively alleviate salt stress, improve root morphology, promote cotton plant growth, and raise water use efficiency and partial factor productivity, which is a promising combined strategy in alleviating drought and salt stress.

CRediT authorship contribution statement

Jingxiang Hou: Experiment execution, data acquisition, data collation, data analysis, manuscript writing, methodology. **Heng Wan:** Experiment assistance, data acquisition and analysis. **Kehao Liang:** Data analysis, manuscript revision. **Bingjing Cui:** Experiment assistance, data acquisition. **Yingying Ma:** Provide guidance on operational specifications, data analysis. **Yiting Chen:** Use of software, data analysis assistance. **Jie Liu:** Provide guidance on the use of instruments and help with experiments. **Yin Wang:** Revision of manuscripts and comments. **Xuezhi Liu:** Data analysis. **Jiarui Zhang:** Data acquisition and collection. **Zhenhua Wei:** Provide guidance and revision of manuscripts. **Fulai Liu:** Conceptualization, methodology, data analysis, evaluation and modification, guidance and management.

Declaration of competing interest

The authors declare that they have no known competing financial interests or personal relationships that could have appeared to influence the work reported in this paper.

Data availability

Data will be made available on request.

Acknowledgements

The authors acknowledge the financial support provided by China Scholarship Council (CSC) to complete his research at the Faculty of Science, University of Copenhagen, Denmark.

Appendix A. Supplementary data

Supplementary data to this article can be found online at https://doi.org/10.1016/j.scitotenv.2023.166978.

References

Abdelraheem, A., Esmaeili, N., O'Connell, M., Zhang, J., 2019. Progress and perspective on drought and salt stress tolerance in cotton. Ind. Crop. Prod. 130, 118–129.
Ahanger, M.A., Agarwal, R.M., 2017. Salinity stress induced alterations in antioxidant metabolism and nitrogen assimilation in wheat (Triticum aestivum L) as influenced by potassium supplementation. Plant Physiol. Biochem. 115, 449–460.
Ahmad, M., Rajapaksha, A.U., Lim, J.E., Zhang, M., Bolan, N., Mohan, D., Vithanage, M., Lee, S.S., Ok, Y.S., 2014. Biochar as a sorbent for contaminant management in soil and water: a review. Chemosphere 99, 19–33.
Ahmed, M.J., Hameed, B.H., 2020. Insight into the co-pyrolysis of different blended feedstocks to biochar for the adsorption of organic and inorganic pollutants: a review. J. Clean. Prod. 265.
Akhtar, S.S., Andersen, M.N., Liu, F., 2015a. Biochar mitigates salinity stress in potato. J. Agron. Crop Sci. 201, 368–378.
Akhtar, S.S., Andersen, M.N., Liu, F., 2015b. Residual effects of biochar on improving growth, physiology and yield of wheat under salt stress. Agric. Water Manag. 158, 61–68.
Akhtar, S.S., Andersen, M.N., Naveed, M., Zahir, Z.A., Liu, F., 2015c. Interactive effect of biochar and plant growth-promoting bacterial endophytes on ameliorating salinity stress in maize. Funct. Plant Biol. 42, 770–781.
Alhaj Hamoud, Y., Shaghaleh, H., Sheteiwy, M., Guo, X., Elshaikh, N.A., Ullah Khan, N., Oumarou, A., Rahim, S.F., 2019. Impact of alternative wetting and soil drying and soil clay content on the morphological and physiological traits of rice roots and their relationships to yield and nutrient use-efficiency. Agric. Water Manag. 223.
Aller, D., Rathke, S., Laird, D., Cruse, R., Hatfield, J., 2017. Impacts of fresh and aged biochars on plant available water and water use efficiency. Geoderma 307, 114–121.
Alvarez, S., Sanchez-Blanco, M.J., 2015. Comparison of individual and combined effects of salinity and deficit irrigation on physiological, nutritional and ornamental aspects of tolerance in Callistemon laevis plants. J. Plant Physiol. 185, 65–74.
Alves, R.C., de Medeiros, A.S., Nicolau, M.C.M., Neto, A.P., de Assis Oliveira, F., Lima, L. W., Tezotto, T., Gratao, P.L., 2018. The partial root-zone saline irrigation system and antioxidant responses in tomato plants. Plant Physiol. Biochem. 127, 366–379.
Ashraf, M., Ahmad, A., McNeilly, T., 2001. Growth and photosynthetic characteristics in pearl millet under water stress and different potassium supply. Photosynthetica 39, 389–394.
Awad, W., Byrne, P.F., Reid, S.D., Comas, L.H., Haley, S.D., 2018. Great Plains winter wheat varies for root length and diameter under drought stress. Agron. J. 110, 226–235.
Awan, S., Ippolito, J.A., Ullman, J.L., Ansari, K., Cui, L., Siyal, A.A., 2020. Biochars reduce irrigation water sodium adsorption ratio. Biochar 3, 77–87.
Backer, R.G.M., Saeed, W., Seguin, P., Smith, D.L., 2017. Root traits and nitrogen fertilizer recovery efficiency of corn grown in biochar-amended soil under greenhouse conditions. Plant Soil 415, 465–477.
Bazihizina, N., Colmer, T.D., Barrett-Lennard, E.G., 2009. Response to non-uniform salinity in the root zone of the halophyte Atriplex nummularia: growth, photosynthesis, water relations and tissue ion concentrations. Ann. Bot. 104, 737–745.
Bekiaris, G., Peltre, C., Jensen, L.S., Bruun, S., 2016. Using FTIR-photoacoustic spectroscopy for phosphorus speciation analysis of biochars. Spectrochim. Acta A Mol. Biomol. Spectrosc. 168, 29–36.
Berthomieu, P., Conejero, G., Nublat, A., Brackenbury, W.J., Lambert, C., Savio, C., Uozumi, N., Oiki, S., Yamada, K., Cellier, F., Gosti, F., Simonneau, T., Essah, P.A., Tester, M., Very, A.A., Sentenac, H., Casse, F., 2003. Functional analysis of AtHKT1 in Arabidopsis shows that Na(+) recirculation by the phloem is crucial for salt tolerance. EMBO J. 22, 2004–2014.

Cai, W., Bordoloi, S., Ng, C.W.W., Sarmah, A.K., 2022. Influence of pore fluid salinity on shrinkage and water retention characteristics of biochar amended kaolin for landfill liner application. Sci. Total Environ. 838, 156493.
Cakmak, I., 2005. The role of potassium in alleviating detrimental effects of abiotic stresses in plants. J. Plant Nutr. Soil Sci. 168, 521–530.
Casenave, E.C., Degano, C.A., Toselli, M.E., Catan, E.A., 1999. Statistical studies on anatomical modifications in the radicle and hypocotyl of cotton induced by NaCl. Biol. Res. 32, 289–295.
Chakraborty, K., Bhaduri, D., Meena, H.N., Kalariya, K., 2016. External potassium (K(+)) application improves salinity tolerance by promoting Na(+)-exclusion, K(+)-accumulation and osmotic adjustment in contrasting peanut cultivars. Plant Physiol. Biochem. 103, 143–153.
Chan, W.P., Wang, J.-Y., 2018. Formation of synthetic sludge as a representative tool for thermochemical conversion modelling and performance analysis of sewage sludge – based on a TG-FTIR study. J. Anal. Appl. Pyrolysis 133, 97–106.
Che, Y., Yao, T., Wang, H., Wang, Z., Zhang, H., Sun, G., Zhang, H., 2022. Potassium ion regulates hormone, Ca(2+) and H(2)O(2) signal transduction and antioxidant activities to improve salt stress resistance in tobacco. Plant Physiol. Biochem. 186, 40–51.
Chen, W., Jin, M., Ferré, T.P.A., Liu, Y., Xian, Y., Shan, T., Ping, X., 2018. Spatial distribution of soil moisture, soil salinity, and root density beneath a cotton field under mulched drip irrigation with brackish and fresh water. Field Crop Res. 215, 207–221.
Chen, W., Jin, M., Ferré, T.P.A., Liu, Y., Huang, J., Xian, Y., 2020. Soil conditions affect cotton root distribution and cotton yield under mulched drip irrigation. Field Crop Res. 249.
Chen, X., Lu, X., Shu, N., Wang, D., Wang, S., Wang, J., Guo, L., Guo, X., Fan, W., Lin, Z., Ye, W., 2017. GhSOS1, a plasma membrane Na+/H+ antiporter gene from upland cotton, enhances salt tolerance in transgenic Arabidopsis thaliana. PLoS One 12, e0181450.
Cheng, N., Peng, Y., Kong, Y., Li, J., Sun, C., 2018. Combined effects of biochar addition and nitrogen fertilizer reduction on the rhizosphere metabolomics of maize (Zea mays L.) seedlings. Plant Soil 433, 19–35.
Chinnusamy, V., Jagendorf, A., Zhu, J.K., 2005. Understanding and improving salt tolerance in plants. Crop Sci. 45, 437–448.
Chun, H.C., Lee, S., Choi, Y.D., Gong, D.H., Jung, K.Y., 2021. Effects of drought stress on root morphology and spatial distribution of soybean and adzuki bean. J. Integr. Agric. 20, 2639–2651.
Dai, J., Duan, L., Dong, H., 2014. Comparative effect of nitrogen forms on nitrogen uptake and cotton growth under salinity stress. J. Plant Nutr. 38, 1530–1543.
Dai, L., Han, T., Ma, G., Tian, X., Meng, K., Lei, Z., Ren, J., 2022. Effective removal of Cd (ii) by sludge biochar supported nanoscale zero-valent iron from aqueous solution: characterization, adsorption properties and mechanism. New J. Chem. 46, 13184–13195.
Davies, W.J., Wilkinson, S., Loveys, B., 2002. Stomatal control by chemical signalling and the exploitation of this mechanism to increase water use efficiency in agriculture. New Phytol. 153, 449–460.
Deliyanni, E., Arabatzidou, A., Tzoupanos, N., Matis, K.A., 2012. Adsorption of Pb2+ using mesoporous activated carbon and its effects on surface modifications. Adsorpt. Sci. Technol. 30, 627–645.
Djanaguiraman, M., Prasad, P.V.V., Kumari, J., Rengel, Z., 2018. Root length and root lipid composition contribute to drought tolerance of winter and spring wheat. Plant Soil 439, 57–73.
Dong, H., Kong, X., Luo, Z., Li, W., Xin, C., 2010. Unequal salt distribution in the root zone increases growth and yield of cotton. Eur. J. Agron. 33, 285–292.
Dong, X., Zhang, Z., Wang, S., Shen, Z., Cheng, X., Lv, X., Pu, X., 2022. Soil properties, root morphology and physiological responses to cotton stalk biochar addition in two continuous cropping cotton field soils from Xinjiang, China. PeerJ 10, e12928.
Drake, J.A., Cavagnaro, T.R., Cunningham, S.C., Jackson, W.R., Patti, A.F., 2015. Does biochar improve establishment of tree seedlings in saline sodic soils? Land Degrad. Dev. 27, 52–59.
Dubinin, M.M., 1975. Physical adsorption of gases and vapors in micropores. In: Cadenhead, D.A., Danielli, J.F., Rosenberg, M.D. (Eds.), Progress in Surface and Membrane Science. Elsevier, pp. 1–70.
Essa, T.A., 2002. Effect of salinity stress on growth and nutrient composition of three soybean (Glycine max L. Merrill) cultivars. J. Agron. Crop Sci. 188, 86–93.
Feng, L., Xu, W., Tang, G., Gu, M., Geng, Z., 2021. Biochar induced improvement in root system architecture enhances nutrient assimilation by cotton plant seedlings. BMC Plant Biol. 21, 269.
Feng, X., An, P., Guo, K., Li, X., Liu, X., Zhang, X., 2017. Growth, root compensation and ion distribution in Lycium chinense under heterogeneous salinity stress. Sci. Hortic. 226, 24–32.
Freundlich, H., 1907. Über die adsorption in lösungen. Z. Phys. Chem. 57, 385–470.
Galvan-Ampudia, C.S., Testerink, C., 2011. Salt stress signals shape the plant root. Curr. Opin. Plant Biol. 14, 296–302.
Graber, E.R., Meller Harel, Y., Kolton, M., Cytryn, E., Silber, A., Rav David, D., Tsechansky, L., Borenshtein, M., Elad, Y., 2010. Biochar impact on development and productivity of pepper and tomato grown in fertigated soilless media. Plant Soil 337, 481–496.
Gray, M., Johnson, M.G., Dragila, M.I., Kleber, M., 2014. Water uptake in biochars: the roles of porosity and hydrophobicity. Biomass Bioenergy 61, 196–205.
Guo, P., Wei, H., Zhang, W., Bao, Y., 2015. Physiological responses of alfalfa to high-level salt stress: root ion flux and stomatal characteristics. Int. J. Agric. Biol. 18, 125–133.
Guo, X., Li, M., Liu, A., Jiang, M., Niu, X., Liu, X., 2020. Adsorption mechanisms and characteristics of Hg2+ removal by different fractions of biochar. Water 12.
Hamada, A., Nitta, M., Nasuda, S., Kato, K., Fujita, M., Matsunaka, H., Okumoto, Y., 2011. Novel QTLs for growth angle of seminal roots in wheat (Triticum aestivum L.). Plant Soil 354, 395–405.
Hammer, E.C., Forstreuter, M., Rillig, M.C., Kohler, J., 2015. Biochar increases arbuscular mycorrhizal plant growth enhancement and ameliorates salinity stress. Appl. Soil Ecol. 96, 114–121.
Hannachi, S., Van Labeke, M.-C., 2018. Salt stress affects germination, seedling growth and physiological responses differentially in eggplant cultivars (Solanum melongena L.). Sci. Hortic. 228, 56–65.
Hasan, M.S., Geza, M., Vasquez, R., Chilkoor, G., Gadhamshetty, V., 2020. Enhanced heavy metal removal from synthetic stormwater using nanoscale zerovalent iron–modified biochar. Water Air Soil Pollut. 231.
Horie, T., Hauser, F., Schroeder, J.I., 2009. HKT transporter-mediated salinity resistance mechanisms in Arabidopsis and monocot crop plants. Trends Plant Sci. 14, 660–668.
Hou, J., Zhang, J., Liu, X., Ma, Y., Wei, Z., Wan, H., Liu, F., 2023. Effect of biochar addition and reduced irrigation regimes on growth, physiology and water use efficiency of cotton plants under salt stress. Ind. Crop. Prod. 198, 116702.
Hu, L., Wang, Z., Huang, B., 2013. Effects of cytokinin and potassium on stomatal and photosynthetic recovery of Kentucky bluegrass from drought stress. Crop Sci. 53, 221–231.
Hu, Y., Schmidhalter, U., 2005. Drought and salinity: a comparison of their effects on mineral nutrition of plants. J. Plant Nutr. Soil Sci. 168, 541–549.
Huang, M., Li, Z., Huang, B., Luo, N., Zhang, Q., Zhai, X., Zeng, G., 2018. Investigating binding characteristics of cadmium and copper to DOM derived from compost and rice straw using EEM-PARAFAC combined with two-dimensional FTIR correlation analyses. J. Hazard. Mater. 344, 539–548.
Huang, M., Zhang, Z., Zhai, Y., Lu, P., Zhu, C., 2019. Effect of straw biochar on soil properties and wheat production under saline water irrigation. Agronomy 9.
Hussain, R., Ravi, K., Garg, A., 2020. Influence of biochar on the soil water retention characteristics (SWRC): potential application in geotechnical engineering structures. Soil Tillage Res. 204.
Jarvis, P., Rey, A., Petsikos, C., Wingate, L., Rayment, M., Pereira, J., Banza, J., David, J., Miglietta, F., Borghetti, M., 2007. Drying and wetting of Mediterranean soils stimulates decomposition and carbon dioxide emission: the "Birch effect". Tree Physiol. 27, 929–940.
Jiang, M., Zhang, J., 2001. Effect of abscisic acid on active oxygen species, antioxidative defence system and oxidative damage in leaves of maize seedlings. Plant Cell Physiol. 42, 1265–1273.
Jing, F., Sun, Y., Liu, Y., Wan, Z., Chen, J., Tsang, D.C.W., 2022. Interactions between biochar and clay minerals in changing biochar carbon stability. Sci. Total Environ. 809, 151124.
Ju, F., Pang, J., Huo, Y., Zhu, J., Yu, K., Sun, L., Loka, D.A., Hu, W., Zhou, Z., Wang, S., Chen, B., Tang, Q., 2021. Potassium application alleviates the negative effects of salt stress on cotton (Gossypium hirsutum L.) yield by improving the ionic homeostasis, photosynthetic capacity and carbohydrate metabolism of the leaf subtending the cotton boll. Field Crop Res. 272.
Ju, F., Pang, J., Sun, L., Gu, J., Wang, Z., Wu, X., Ali, S., Wang, Y., Zhao, W., Wang, S., Zhou, Z., Chen, B., 2023. Integrative transcriptomic, metabolomic and physiological analyses revealed the physiological and molecular mechanisms by which potassium regulates the salt tolerance of cotton (Gossypium hirsutum L.) roots. Ind. Crop. Prod. 193.
Kamran, M., Malik, Z., Parveen, A., Zong, Y., Abbasi, G.H., Rafiq, M.T., Shaaban, M., Mustafa, A., Bashir, S., Rafay, M., Mehmood, S., Ali, M., 2019. Biochar alleviates Cd phytotoxicity by minimizing bioavailability and oxidative stress in pak choi (Brassica chinensis L.) cultivated in Cd-polluted soil. J. Environ. Manag. 250, 109500.
Kang, S., Zhang, J., 2004. Controlled alternate partial root-zone irrigation: its physiological consequences and impact on water use efficiency. J. Exp. Bot. 55, 2437–2446.
Kashiwagi, J., Krishnamurthy, L., Crouch, J.H., Serraj, R., 2006. Variability of root length density and its contributions to seed yield in chickpea (Cicer arietinum L.) under terminal drought stress. Field Crop Res. 95, 171–181.
Kataki, S., Hazarika, S., Baruah, D.C., 2017. Investigation on by-products of bioenergy systems (anaerobic digestion and gasification) as potential crop nutrient using FTIR, XRD, SEM analysis and phyto-toxicity test. J. Environ. Manag. 196, 201–216.
Kiani, D., Soltanloo, H., Ramezanpour, S.S., Nasrolahnezhad Qumi, A.A., Yamchi, A., Zaynali Nezhad, K., Tavakol, E., 2017. A barley mutant with improved salt tolerance through ion homeostasis and ROS scavenging under salt stress. Acta Physiol. Plant. 39.
Kim, H.S., Kim, K.R., Yang, J.E., Ok, Y.S., Owens, G., Nehls, T., Wessolek, G., Kim, K.H., 2016. Effect of biochar on reclaimed tidal land soil properties and maize (Zea mays L.) response. Chemosphere 142, 153–159.
Kong, X., Luo, Z., Dong, H., Eneji, A.E., Li, W., 2012. Effects of non-uniform root zone salinity on water use, Na+ recirculation, and Na+ and H+ flux in cotton. J. Exp. Bot. 63, 2105–2116.
Kong, X., Luo, Z., Dong, H., Eneji, A.E., Li, W., 2016. H2O2 and ABA signaling are responsible for the increased Na+ efflux and water uptake in Gossypium hirsutum L. roots in the non-saline side under non-uniform root zone salinity. J. Exp. Bot. 67, 2247–2261.
Kong, X., Luo, Z., Dong, H., Li, W., Chen, Y., 2017. Non-uniform salinity in the root zone alleviates salt damage by increasing sodium, water and nutrient transport genes expression in cotton. Sci. Rep. 7, 2879.
Koushafar, M., Khoshgoftarmanesh, A.H., Moezzi, A., Mobli, M., 2011. Effect of dynamic unequal distribution of salts in the root environment on performance and Crop Per Drop (CPD) of hydroponic-grown tomato. Sci. Hortic. 131, 1–5.
Kozyatnyk, I., Oesterle, P., Wurzer, C., Masek, O., Jansson, S., 2021. Removal of contaminants of emerging concern from multicomponent systems using carbon

dioxide activated biochar from lignocellulosic feedstocks. Bioresour. Technol. 340, 125561.
Lai, D., Mao, Y., Zhou, H., Li, F., Wu, M., Zhang, J., He, Z., Cui, W., Xie, Y., 2014. Endogenous hydrogen sulfide enhances salt tolerance by coupling the reestablishment of redox homeostasis and preventing salt-induced K(+) loss in seedlings of Medicago sativa. Plant Sci. 225, 117–129.
Langmuir, I., 1918. The adsorption of gases on plane surfaces of glass, mica and platinum. J. Am. Chem. Soc. 40, 1361–1403.
Leng, L., Liu, R., Xu, S., Mohamed, B.A., Yang, Z., Hu, Y., Chen, J., Zhao, S., Wu, Z., Peng, H., Li, H., Li, H., 2022. An overview of sulfur-functional groups in biochar from pyrolysis of biomass. J. Environ. Chem. Eng. 10.
Li, H., Sun, H., Ping, W., Liu, L., Zhang, Y., Zhang, K., Bai, Z., Li, A., Zhu, J., Li, C., 2023. Exogenous ethylene promotes the germination of cotton seeds under salt stress. J. Plant Growth Regul. 42, 3923–3933.
Li, C., Xiong, Y., Qu, Z., Xu, X., Huang, Q., Huang, G., 2018a. Impact of biochar addition on soil properties and water-fertilizer productivity of tomato in semi-arid region of Inner Mongolia, China. Geoderma 331, 100–108.
Li, Q.W., Liang, J.F., Zhang, X.Y., Feng, J.G., Song, M.H., Gao, J.Q., 2021. Biochar addition affects root morphology and nitrogen uptake capacity in common reed (Phragmites australis). Sci. Total Environ. 766, 144381.
Li, T., Yang, X., Lu, L., Islam, E., He, Z., 2009. Effects of zinc and cadmium interactions on root morphology and metal translocation in a hyperaccumulating species under hydroponic conditions. J. Hazard. Mater. 169, 734–741.
Li, X., Kang, S., Zhang, X., Li, F., Lu, H., 2018b. Deficit irrigation provokes more pronounced responses of maize photosynthesis and water productivity to elevated CO 2. Agric. Water Manag. 195, 71–83.
Li, Y., Yao, N., Liang, J., Wang, X., Niu, B., Jia, Y., Jiang, F., Yu, Q., Liu, D.L., Feng, H., He, H., Yang, G., Pulatov, A., 2023. Rational biochar application rate for cotton nutrient content, growth, yields, productivity, and economic benefits under film-mulched trickle irrigation. Agric. Water Manag. 276.
Li, Z., Qi, X., Fan, X., Wu, H., Du, Z., Li, P., Lü, M., 2015. Influences of biochars on growth, yield, water use efficiency and root morphology of winter wheat. Trans. Chin. Soc. Agric. Eng. 31, 119–124.
Liang, W., Ma, X., Wan, P., Liu, L., 2018. Plant salt-tolerance mechanism: a review. Biochem. Biophys. Res. Commun. 495, 286–291.
Liao, Z., Zeng, H., Fan, J., Lai, Z., Zhang, C., Zhang, F., Wang, H., Cheng, M., Guo, J., Li, Z., Wu, P., 2022. Effects of plant density, nitrogen rate and supplemental irrigation on photosynthesis, root growth, seed yield and water-nitrogen use efficiency of soybean under ridge-furrow plastic mulching. Agric. Water Manag. 268.
Liu, B., Peng, X., Han, L., Hou, L., Li, B., 2020. Effects of exogenous spermidine on root metabolism of cucumber seedlings under salt stress by GC-MS. Agronomy 10.
Liu, C., Yin, Z., Hu, D., Mo, F., Chu, R., Zhu, L., Hu, C., 2021a. Biochar derived from chicken manure as a green adsorbent for naphthalene removal. Environ. Sci. Pollut. Res. Int. 28, 36585–36597.
Liu, F., Shahnazari, A., Andersen, M.N., Jacobsen, S.E., Jensen, C.R., 2006. Physiological responses of potato (Solanum tuberosum L.) to partial root-zone drying: ABA signalling, leaf gas exchange, and water use efficiency. J. Exp. Bot. 57, 3727–3735.
Liu, X., Wei, Z., Ma, Y., Liu, J., Liu, F., 2021b. Effects of biochar amendment and reduced irrigation on growth, physiology, water-use efficiency and nutrients uptake of tobacco (Nicotiana tabacum L.) on two different soil types. Sci. Total Environ. 770, 144769.
Liu, X., Wei, Z., Manevski, K., Liu, J., Ma, Y., Andersen, M.N., Liu, F., 2021c. Partial root-zone drying irrigation increases water-use efficiency of tobacco plants amended with biochar. Ind. Crop. Prod. 166.
Liu, X., Li, G., Chen, C., Zhang, X., Zhou, K., Long, X., 2022a. Banana stem and leaf biochar as an effective adsorbent for cadmium and lead in aqueous solution. Sci. Rep. 12.
Liu, X., Ma, Y., Manevski, K., Andersen, M.N., Li, Y., Wei, Z., Liu, F., 2022b. Biochar and alternate wetting-drying cycles improving rhizosphere soil nutrients availability and tobacco growth by altering root growth strategy in Ferralsol and Anthrosol. Sci. Total Environ. 806, 150513.
Lu, H., Zhang, W., Yang, Y., Huang, X., Wang, S., Qiu, R., 2012. Relative distribution of Pb2+ sorption mechanisms by sludge-derived biochar. Water Res. 46, 854–862.
Ma, Y., Wei, Z., Liu, J., Liu, X., Hou, J., Liu, F., 2021. Effects of K+ and Ca2+ supplement during fertigation on leaf gas exchange and salt tolerance of cotton at full and deficit irrigation regimes. Environ. Exp. Bot. 186.
Ma, Z., Ren, B., Zhao, B., Liu, P., Zhang, J., 2022. Optimising the root traits of summer maize to improve nutrient uptake and utilisation through rational application of urea ammonium nitrate solution. Plant Soil Environ. 68, 98–107.
Mahmoud, E., Ibrahim, M., Ali, N., Ali, H., 2020. Effect of biochar and compost amendments on soil biochemical properties and dry weight of canola plant grown in soil contaminated with heavy metals. Commun. Soil Sci. Plant Anal. 51, 1561–1571.
Malik, R., Dahiya, S., Lata, S., 2017. An experimental and quantum chemical study of removal of utmostly quantified heavy metals in wastewater using coconut husk: a novel approach to mechanism. Int. J. Biol. Macromol. 98, 139–149.
Mane, V.S., Deo Mall, I., Chandra Srivastava, V., 2007. Kinetic and equilibrium isotherm studies for the adsorptive removal of Brilliant Green dye from aqueous solution by rice husk ash. J. Environ. Manag. 84, 390–400.
Margenot, A.J., Calderón, F.J., Parikh, S.J., 2016. Limitations and potential of spectral subtractions in Fourier-transform infrared spectroscopy of soil samples. Soil Sci. Soc. Am. J. 80, 10–26.
Marks, E.A.N., Mattana, S., Alcañiz, J.M., Pérez-Herrero, E., Domene, X., 2016. Gasifier biochar effects on nutrient availability, organic matter mineralization, and soil fauna activity in a multi-year Mediterranean trial. Agric. Ecosyst. Environ. 215, 30–39.
Mehmood, S., Ahmed, W., Ikram, M., Imtiaz, M., Mahmood, S., Tu, S., Chen, D., 2020. Chitosan modified biochar increases soybean (Glycine max L.) resistance to salt-stress by augmenting root morphology, antioxidant defense mechanisms and the expression of stress-responsive genes. Plants (Basel) 9.
Min, W., Guo, H., Zhou, G., Zhang, W., Ma, L., Ye, J., Hou, Z., 2014. Root distribution and growth of cotton as affected by drip irrigation with saline water. Field Crop Res. 169, 1–10.
Mireles, S., Parsons, J., Trad, T., Cheng, C.L., Kang, J., 2019. Lead removal from aqueous solutions using biochars derived from corn stover, orange peel, and pistachio shell. Int. J. Environ. Sci. Technol. 16, 5817–5826.
Moradi, S., Rasouli-Sadaghiani, M.H., Sepehr, E., Khodaverdiloo, H., Barin, M., 2019. Soil nutrients status affected by simple and enriched biochar application under salinity conditions. Environ. Monit. Assess. 191, 257.
Moussavi, G., Khosravi, R., 2012. Preparation and characterization of a biochar from pistachio hull biomass and its catalytic potential for ozonation of water recalcitrant contaminants. Bioresour. Technol. 119, 66–71.
Mulholland, B.J., Fussell, M., Edmondson, R.N., Taylor, A.J., Basham, J., McKee, J.M.T., Parsons, N., 2015. The effect of split-root salinity stress on tomato leaf expansion, fruit yield and quality. J. Hortic. Sci. Biotechnol. 77, 509–519.
Munns, R., 2002. Comparative physiology of salt and water stress. Plant Cell Environ. 25, 239–250.
Munns, R., Tester, M., 2008. Mechanisms of salinity tolerance. Annu. Rev. Plant Biol. 59, 651–681.
Nair, R.R., Mondal, M.M., Weichgrebe, D., 2020. Biochar from co-pyrolysis of urban organic wastes—investigation of carbon sink potential using ATR-FTIR and TGA. Biomass Convers. Biorefin. 12, 4729–4743.
Nguyen, B.T., Dinh, G.D., Dong, H.P., Le, L.B., 2022. Sodium adsorption isotherm and characterization of biochars produced from various agricultural biomass wastes. J. Clean. Prod. 346.
Nguyen, T.T.N., Xu, C.-Y., Tahmasbian, I., Che, R., Xu, Z., Zhou, X., Wallace, H.M., Bai, S. H., 2017. Effects of biochar on soil available inorganic nitrogen: a review and meta-analysis. Geoderma 288, 79–96.
Oram, N.J., van de Voorde, T.F.J., Ouwehand, G.-J., Bezemer, T.M., Mommer, L., Jeffery, S., Groenigen, J.W.V., 2014. Soil amendment with biochar increases the competitive ability of legumes via increased potassium availability. Agric. Ecosyst. Environ. 191, 92–98.
Ostonen, I., Püttsepp, Ü., Biel, C., Alberton, O., Bakker, M.R., Lõhmus, K., Majdi, H., Metcalfe, D., Olsthoorn, A.F.M., Pronk, A., Vanguelova, E., Weih, M., Brunner, I., 2007. Specific root length as an indicator of environmental change. Plant Biosyst. 141, 426–442.
Pahlavan, F., Ghasemi, H., Yazdani, H., Fini, E.H., 2023. Soil amended with algal biochar reduces mobility of deicing salt contaminants in the environment: an atomistic insight. Chemosphere 323, 138172.
Palomino, A.M., Santamarina, J.C., 2005. Fabric map for kaolinite: effects of pH and ionic concentration on behavior. Clay Clay Miner. 53, 211–223.
Pardo, J.M., 2010. Biotechnology of water and salinity stress tolerance. Curr. Opin. Biotechnol. 21, 185–196.
Parkash, V., Singh, S., 2020. Potential of biochar application to mitigate salinity stress in eggplant. HortScience 55, 1946–1955.
Philippar, K., Ivashikina, N., Ache, P., Christian, M., Luthen, H., Palme, K., Hedrich, R., 2004. Auxin activates KAT1 and KAT2, two K+-channel genes expressed in seedlings of Arabidopsis thaliana. Plant J. 37, 815–827.
Purakayastha, T.J., Kumari, S., Pathak, H., 2015. Characterisation, stability, and microbial effects of four biochars produced from crop residues. Geoderma 239-240, 293–303.
Qiu, B., Shao, Q., Shi, J., Yang, C., Chu, H., 2022. Application of biochar for the adsorption of organic pollutants from wastewater: modification strategies, mechanisms and challenges. Sep. Purif. Technol. 300.
Qiu, Q.-S., Guo, Y., Dietrich, M.A., Schumaker, K.S., Zhu, J.-K., 2002. Regulation of SOS1, a plasma membrane Na+/H+ exchanger in Arabidopsis thaliana, by SOS2 and SOS3. Proc. Natl. Acad. Sci. 99, 8436–8441.
Rajapaksha, A.U., Chen, S.S., Tsang, D.C., Zhang, M., Vithanage, M., Mandal, S., Gao, B., Bolan, N.S., Ok, Y.S., 2016. Engineered/designer biochar for contaminant removal/immobilization from soil and water: potential and implication of biochar modification. Chemosphere 148, 276–291.
Ranjan, A., Sinha, R., Singla-Pareek, S.L., Pareek, A., Singh, A.K., 2022. Shaping the root system architecture in plants for adaptation to drought stress. Physiol. Plant. 174, e13651.
Raynaud, X., Leadley, P.W., 2004. Soil characteristics play a key role in modeling nutrient competition in plant communities. Ecology 85, 2200–2214.
Ren, Z., Shi, J., Guo, A., Wang, Y., Fan, X., Li, R., Yu, C., Peng, Z., Gao, Y., Liu, Z., Duan, L., 2022. Melatonin mediates the regulation of morphological and anatomical traits in Carex leucochlora under continuous salt stress. Agronomy 12.
Rewald, B., Raveh, E., Gendler, T., Ephrath, J.E., Rachmilevitch, S., 2012. Phenotypic plasticity and water flux rates of Citrus root orders under salinity. J. Exp. Bot. 63, 2717–2727.
Rewald, B., Shelef, O., Ephrath, J.E., Rachmilevitch, S., 2013. Adaptive plasticity of salt-stressed root systems. In: Ahmad, P., Azooz, M.M., Prasad, M.N.V. (Eds.), Ecophysiology and Responses of Plants under Salt Stress. Springer New York, New York, NY, pp. 169–201.
Rostamian, R., Heidarpour, M., Mousavi, S.F., Afyuni, M., 2018. Characterization and Sodium Sorption Capacity of Biochar and Activated Carbon Prepared From Rice Hus.
Ruan, X., Sun, Y., Du, W., Tang, Y., Liu, Q., Zhang, Z., Doherty, W., Frost, R.L., Qian, G., Tsang, D.C.W., 2019. Formation, characteristics, and applications of environmentally persistent free radicals in biochars: a review. Bioresour. Technol. 281, 457–468.

Sahoo, K., Kumar, A., Chakraborty, J.P., 2020. A comparative study on valuable products: bio-oil, biochar, non-condensable gases from pyrolysis of agricultural residues. J. Mater. Cycles Waste Manag. 23, 186–204.
Salam, A., Bashir, S., Khan, I., Hu, H., 2020. Biochar production and characterization as a measure for effective rapeseed residue and rice straw management: an integrated spectroscopic examination. Biomass Convers. Biorefin. 12, 2687–2696.
Sangakkara, U.R., Frehner, M., Nosberger, J., 2000. Effect of soil moisture and potassium fertilizer on shoot water potential, photosynthesis and partitioning of carbon in mungbean and cowpea. J. Agron. Crop Sci. 185, 201–207.
Shabala, S., Pottosin, I., 2014. Regulation of potassium transport in plants under hostile conditions: implications for abiotic and biotic stress tolerance. Physiol. Plant. 151, 257–279.
Shen, Z., Zhang, Y., McMillan, O., Jin, F., Al-Tabbaa, A., 2017. Characteristics and mechanisms of nickel adsorption on biochars produced from wheat straw pellets and rice husk. Environ. Sci. Pollut. Res. Int. 24, 12809–12819.
Shu, L.-Z., Liu, R., Min, W., Wang, Y.-S., Hong-Mei, Y., Zhu, P.-F., Zhu, J.-R., 2020. Regulation of soil water threshold on tomato plant growth and fruit quality under alternate partial root-zone drip irrigation. Agric. Water Manag. 238.
Siddiqui, M.N., Leon, J., Naz, A.A., Ballvora, A., 2021. Genetics and genomics of root system variation in adaptation to drought stress in cereal crops. J. Exp. Bot. 72, 1007–1019.
Sonneveld, C., de Kreij, C., 1999. Response of cucumber (Cucumis sativus L.) to an unequal distribution of salts in the root environment. Plant Soil 209, 47–56.
Soria, R.I., Rolfe, S.A., Betancourth, M.P., Thornton, S.F., 2020. The relationship between properties of plant-based biochars and sorption of Cd(II), Pb(II) and Zn(II) in soil model systems. Heliyon 6, e05388.
Spokas, K.A., Novak, J.M., Stewart, C.E., Cantrell, K.B., Uchimiya, M., Dusaire, M.G., Ro, K.S., 2011. Qualitative analysis of volatile organic compounds on biochar. Chemosphere 85, 869–882.
Srivastava, S., Agrawal, S.B., Mondal, M.K., 2015. Biosorption isotherms and kinetics on removal of Cr(VI) using native and chemically modified Lagerstroemia speciosa bark. Ecol. Eng. 85, 56–66.
Sun, H.N., Wang, S.W., Li, Y.L., Yang, W.J., Yin, X.S., Yin, L.N., Deng, X.P., 2018. Effects of biochar levels on winter wheat yield and water-use efficiency in Loess Plateau. Agric. Res. Arid Areas. 36, 159–167.
Sun, J., Yang, G., Zhang, W., Zhang, Y., 2016. Effects of heterogeneous salinity on growth, water uptake, and tissue ion concentrations of alfalfa. Plant Soil 408, 211–226.
Sun, J., Yang, R., Li, Y., Geng, Y., Pan, Y., Zhang, Z., 2022. Fading positive effect of biochar on cotton yield in a coastal saline soil during a 2-year field trial. J. Soil Sci. Plant Nutr. 23, 991–1002.
Sun, Y., Xiong, X., He, M., Xu, Z., Hou, D., Zhang, W., Ok, Y.S., Rinklebe, J., Wang, L., Tsang, D.C.W., 2021. Roles of biochar-derived dissolved organic matter in soil amendment and environmental remediation: a critical review. Chem. Eng. J. 424.
Taha, A.A., Ahmed, A.M., Abdel Rahman, H.H., Abouzeid, F.M., Abdel Maksoud, M.O., 2016. Removal of nickel ions by adsorption on nano-bentonite: equilibrium, kinetics, and thermodynamics. J. Dispers. Sci. Technol. 38, 757–767.
Tang, J., Zhuang, L., Yu, Z., Liu, X., Wang, Y., Wen, P., Zhou, S., 2019. Insight into complexation of Cu(II) to hyperthermophilic compost-derived humic acids by EEM-PARAFAC combined with heterospectral two dimensional correlation analyses. Sci. Total Environ. 656, 29–38.
Tang, J., Zhang, S., Zhang, X., Chen, J., He, X., Zhang, Q., 2020. Effects of pyrolysis temperature on soil-plant-microbe responses to *Solidago canadensis* L.-derived biochar in coastal saline-alkali soil. Sci. Total Environ. 731, 138938.
Thomas, S.C., Frye, S., Gale, N., Garmon, M., Launchbury, R., Machado, N., Melamed, S., Murray, J., Petroff, A., Winsborough, C., 2013. Biochar mitigates negative effects of salt additions on two herbaceous plant species. J. Environ. Manag. 129, 62–68.
Trakal, L., Bingol, D., Pohorely, M., Hruska, M., Komarek, M., 2014. Geochemical and spectroscopic investigations of Cd and Pb sorption mechanisms on contrasting biochars: engineering implications. Bioresour. Technol. 171, 442–451.
Wang, B., Li, P.P., Huang, C.H., Liu, G.B., Yang, Y.F., 2021a. Effects of root morphological traits on soil detachment for ten herbaceous species in the Loess Plateau. Sci. Total Environ. 754, 142304.
Wang, C., Shu, L., Zhou, S., Yu, H., Zhu, P., 2019a. Effects of alternate partial root-zone irrigation on the utilization and movement of nitrates in soil by tomato plants. Sci. Hortic. 243, 41–47.
Wang, L., Ok, Y.S., Tsang, D.C.W., Alessi, D.S., Rinklebe, J., Mašek, O., Bolan, N.S., Hou, D., 2021b. Biochar composites: emerging trends, field successes and sustainability implications. Soil Use Manag. 38, 14–38.
Wang, M., Zheng, Q., Shen, Q., Guo, S., 2013. The critical role of potassium in plant stress response. Int. J. Mol. Sci. 14, 7370–7390.
Wang, T., Stewart, C.E., Sun, C., Wang, Y., Zheng, J., 2018. Effects of biochar addition on evaporation in the five typical Loess Plateau soils. Catena 162, 29–39.
Wang, Y., Liu, F., Jensen, C.R., 2012. Comparative effects of deficit irrigation and alternate partial root-zone irrigation on xylem pH, ABA and ionic concentrations in tomatoes. J. Exp. Bot. 63, 1907–1917.
Wang, Y., Peng, S., Huang, J., Zhang, Y., Feng, L., Zhao, W., Qi, H., Zhou, G., Deng, N., 2022. Prospects for cotton self-sufficiency in China by closing yield gaps. Eur. J. Agron. 133.
Wang, Z., Wang, J., Xie, L., Zhu, H., Shu, X., 2019b. Influence of the addition of cotton stalk during co-pyrolysis with sewage sludge on the properties, surface characteristics, and ecological risks of biochars. J. Therm. Sci. 28, 755–762.
Wei, Z., Du, T., Li, X., Fang, L., Liu, F., 2018. Interactive effects of CO2 concentration elevation and nitrogen fertilization on water and nitrogen use efficiency of tomato grown under reduced irrigation regimes. Agric. Water Manag. 202, 174–182.
Wu, X., Wang, D., Riaz, M., Zhang, L., Jiang, C., 2019. Investigating the effect of biochar on the potential of increasing cotton yield, potassium efficiency and soil environment. Ecotoxicol. Environ. Saf. 182, 109451.
Xiao, S., Liu, L., Zhang, Y., Sun, H., Zhang, K., Bai, Z., Dong, H., Li, C., 2020. Fine root and root hair morphology of cotton under drought stress revealed with RhizoPot. J. Agron. Crop Sci. 206, 679–693.
Xiong, X., Liu, N., Wei, Y.Q., Bi, Y.X., Luo, J.C., Xu, R.X., Zhou, J.Q., Zhang, Y.J., 2018. Effects of non-uniform root zone salinity on growth, ion regulation, and antioxidant defense system in two alfalfa cultivars. Plant Physiol. Biochem. 132, 434–444.
Xiong, X., Wei, Y.Q., Chen, J.H., Liu, N., Zhang, Y.J., 2020. Transcriptome analysis of genes and pathways associated with salt tolerance in alfalfa under non-uniform salt stress. Plant Physiol. Biochem. 151, 323–333.
Xu, X., Wang, J., Tang, Y., Cui, X., Hou, D., Jia, H., Wang, S., Guo, L., Wang, J., Lin, A., 2023. Mitigating soil salinity stress with titanium gypsum and biochar composite materials: improvement effects and mechanism. Chemosphere 321, 138127.
Yang, A., Akhtar, S.S., Li, L., Fu, Q., Li, Q., Naeem, M.A., He, X., Zhang, Z., Jacobsen, S.-E., 2020. Biochar mitigates combined effects of drought and salinity stress in Quinoa. Agronomy 10.
Yang, F., Xu, Z., Huang, Y., Tsang, D.C.W., Ok, Y.S., Zhao, L., Qiu, H., Xu, X., Cao, X., 2021. Stabilization of dissolvable biochar by soil minerals: release reduction and organo-mineral complexes formation. J. Hazard. Mater. 412, 125213.
Yang, G.X., Jiang, H., 2014. Amino modification of biochar for enhanced adsorption of copper ions from synthetic wastewater. Water Res. 48, 396–405.
Yoshimura, K., Masuda, A., Kuwano, M., Yokota, A., Akashi, K., 2008. Programmed proteome response for drought avoidance/tolerance in the root of a C(3) xerophyte (wild watermelon) under water deficits. Plant Cell Physiol. 49, 226–241.
Yue, Y., Zhang, M., Zhang, J., Duan, L., Li, Z., 2012. SOS1 gene overexpression increased salt tolerance in transgenic tobacco by maintaining a higher K(+)/Na(+) ratio. J. Plant Physiol. 169, 255–261.
Zekri, M., Parsons, L.R., 1990. Response of split-root sour orange seedlings to NaCl and polyethylene glycol stresses1. J. Exp. Bot. 41, 35–40.
Zhang, H., Wang, R., Wang, H., Liu, B., Xu, M., Guan, Y., Yang, Y., Qin, L., Chen, E., Li, F., Huang, R., Zhou, Y., 2019a. Heterogeneous root zone salinity mitigates salt injury to *Sorghum bicolor* (L.) Moench in a split-root system. PLoS One 14, e0227020.
Zhang, J., Bai, Z., Huang, J., Hussain, S., Zhao, F., Zhu, C., Zhu, L., Cao, X., Jin, Q., 2019b. Biochar alleviated the salt stress of induced saline paddy soil and improved the biochemical characteristics of rice seedlings differing in salt tolerance. Soil Tillage Res. 195.
Zhang, J.L., Shi, H., 2013. Physiological and molecular mechanisms of plant salt tolerance. Photosynth. Res. 115, 1–22.
Zhang, J.-L., Flowers, T.J., Wang, S.-M., 2009. Mechanisms of sodium uptake by roots of higher plants. Plant Soil 326, 45–60.
Zhang, P., Chen, Y.-P., Wang, W., Shen, Y., Guo, J.-S., 2016. Surface plasmon resonance for water pollutant detection and water process analysis. TrAC Trends Anal. Chem. 85, 153–165.
Zhang, Q., Wu, S., Chen, C., Shu, L.-Z., Zhou, X.-J., Zhu, S.-N., 2014. Regulation of nitrogen forms on growth of eggplant under partial root-zone irrigation. Agric. Water Manag. 142, 56–65.
Zhang, W.D., Wang, P., Bao, Z., Ma, Q., Duan, L.J., Bao, A.K., Zhang, J.L., Wang, S.M., 2017. SOS1, HKT1;5, and NHX1 synergistically modulate Na(+) homeostasis in the halophytic grass Puccinellia tenuiflora. Front. Plant Sci. 8, 576.
Zhang, X., Cai, X., Wang, Z., Yang, X., Li, S., Liang, G., Xie, X., 2021. Insight into metal binding properties of biochar-derived DOM using EEM-PARAFAC and differential absorption spectra combined with two-dimensional correlation spectroscopy. Environ. Sci. Pollut. Res. Int. 28, 13375–13393.
Zhang, Y., Fang, J., Wu, X., Dong, L., 2018. Na(+)/K(+) balance and transport regulatory mechanisms in weedy and cultivated rice (Oryza sativa L.) under salt stress. BMC Plant Biol. 18, 375.
Zhang, Y., Yang, J., Yao, R., Wang, X., Xie, W., 2020. Short-term effects of biochar and gypsum on soil hydraulic properties and sodicity in a saline-alkali soil. Pedosphere 30, 694–702.
Zheng, N., Yu, Y., Li, Y., Ge, C., Chapman, S.J., Yao, H., 2022. Can aged biochar offset soil greenhouse gas emissions from crop residue amendments in saline and non-saline soils under laboratory conditions? Sci. Total Environ. 806, 151256.
Zhou, M., Bai, W., Li, Q., Guo, Y., Zhang, W.H., 2021. Root anatomical traits determined leaf-level physiology and responses to precipitation change of herbaceous species in a temperate steppe. New Phytol. 229, 1481–1491.
Zhu, Y., Yi, B., Yuan, Q., Wu, Y., Wang, M., Yan, S., 2018. Removal of methylene blue from aqueous solution by cattle manure-derived low temperature biochar. RSC Adv. 8, 19917–19929.